Ontario

Ontario Geological Survey
Open File Report 6134

# Petrography, Chemistry and Diamond Characteristics of Heterolithic Breccia and Lamprophyre Dikes at Wawa, Ontario

2004

Ontario

ONTARIO GEOLOGICAL SURVEY

Open File Report 6134

# Petrography, Chemistry and Diamond Characteristics of Heterolithic Breccia and Lamprophyre Dikes at Wawa, Ontario

by

D. Stone and L. Semenyna

2004

Parts of this publication may be quoted if credit is given. It is recommended that reference to this publication be made in the following form:

Stone, D. and Semenyna, L. 2004. Petrography, chemistry and diamond characteristics of heterolithic breccia and lamprophyre dikes at Wawa, Ontario; Ontario Geological Survey, Open File Report 6134, 39p.

© Queen's Printer for Ontario, 2004

104-04999/

© Queen's Printer for Ontario, 2004.

Open File Reports of the Ontario Geological Survey are available for viewing at the Mines Library in Sudbury, at the Mines and Minerals Information Centre in Toronto, and at the regional Mines and Minerals office whose district includes the area covered by the report (see below).

Copies can be purchased at Publication Sales and the office whose district includes the area covered by the report. Although a particular report may not be in stock at locations other than the Publication Sales office in Sudbury, they can generally be obtained within 3 working days. All telephone, fax, mail and e-mail orders should be directed to the Publication Sales office in Sudbury. Use of VISA or MasterCard ensures the fastest possible service. Cheques or money orders should be made payable to the *Minister of Finance*.

| | | |
|---|---|---|
| Mines and Minerals Information Centre (MMIC)<br>Macdonald Block, Room M2-17<br>900 Bay St.<br>Toronto, Ontario M7A 1C3 | Tel: | (416) 314-3800 |
| Mines Library<br>933 Ramsey Lake Road, Level A3<br>Sudbury, Ontario P3E 6B5 | Tel: | (705) 670-5615 |
| Publication Sales<br>933 Ramsey Lake Rd., Level A3<br>Sudbury, Ontario P3E 6B5 | Tel:<br><br>Fax:<br>E-mail: | (705) 670-5691(local)<br>1-888-415-9845(toll-free)<br>(705) 670-5770<br>pubsales@ndm.gov.on.ca |

**Regional Mines and Minerals Offices:**

Kenora - Suite 104, 810 Robertson St., Kenora P9N 4J2

Kirkland Lake - 10 Government Rd. E., Kirkland Lake P2N 1A8

Red Lake - Box 324, Ontario Government Building, Red Lake P0V 2M0

Sault Ste. Marie - 70 Foster Dr., Ste. 200, Sault Ste. Marie P6A 6V8

Southern Ontario - P.O. Bag Service 43, 126 Old Troy Rd., Tweed K0K 3J0

Sudbury - Level B3, 933 Ramsey Lake Rd., Sudbury P3E 6B5

Thunder Bay - Suite B002, 435 James St. S., Thunder Bay P7E 6S7

Timmins - Ontario Government Complex, P.O. Bag 3060, Hwy. 101 East, South Porcupine P0N 1H0

Toronto - MMIC, Macdonald Block, Room M2-17, 900 Bay St., Toronto M7A 1C3

This report has not received a technical edit. Discrepancies may occur for which the Ontario Ministry of Northern Development and Mines does not assume any liability. Source references are included in the report and users are urged to verify critical information. Recommendations and statements of opinions expressed are those of the author or authors and are not to be construed as statements of government policy.

If you wish to reproduce any of the text, tables or illustrations in this report, please write for permission to the Team Leader, Publication Services, Ministry of Northern Development and Mines, 933 Ramsey Lake Road, Level B4, Sudbury, Ontario P3E 6B5.

**Cette publication est disponible en anglais seulement.**

Parts of this report may be quoted if credit is given. It is recommended that reference be made in the following form:

**Stone, D. and Semenyna, L. 2004. Petrography, chemistry and diamond characteristics of heterolithic breccia and lamprophyre dikes at Wawa, Ontario; Ontario Geological Survey, Open File Report 6134, 39p.**

# Contents


Abstract ..... ix

Introduction ..... 1

Regional Geology ..... 1

Foliated Lamprophyre Dikes and Heterolithic Breccias: Outcrop Characteristics ..... 5

Petrography ..... 6
- Lamprophyre Dikes ..... 8
- Breccia Matrix ..... 8
- Heterolithic Breccia ..... 12
- Ultramafic Xenolith ..... 12
- Diabase Dike ..... 12

Mineral Chemistry ..... 12
- Feldspar ..... 20
- Amphibole ..... 20
- Mica ..... 20
- Pyroxene ..... 20
- Chlorite ..... 20

Rock Chemistry ..... 23

Metamorphism ..... 28

Heavy Mineral and Diamond Processing ..... 30
- Diamond Characteristics ..... 32
- Morphology and Colour of Diamond Grains ..... 32

Summary ..... 34

Acknowledgements ..... 35

References ..... 36

Metric Conversion Table ..... 39


## FIGURES


1. Geology, volcanic cycles and sample locations in the Michipicoten greenstone belt ..... 2
2. Matrix of a lamprophyre dike ..... 9
3. Matrix of heterolithic breccia ..... 11
4. Heterolithic breccia ..... 13
5. Composition of amphiboles ..... 21
6. Composition of mica ..... 22

7. Composition of pyroxene ..... 22
8. Composition of chlorite ..... 23
9. Major element characteristics of breccia and lamprophyre ..... 25
10. Trace element characteristics of breccia and lamprophyre ..... 27
11. P-T conditions of metamorphism of breccia and lamprophyre ..... 29
12. Diamond grains from the Engagement occurrence ..... 31

## TABLES

1. Sample description and disposition ..... 7
2. Mineral assemblages ..... 10
3. Feldspar analyses ..... 14
4. Amphibole analyses ..... 15
5. Mica analyses ..... 17
6. Pyroxene analyses ..... 18
7. Chlorite analyses ..... 19
8. Rock chemistry ..... 24
9. Diamond processing ..... 30
10. Diamond characteristics ..... 33
11. Comparison of lamprophyres with breccia matrix ..... 35

# Abstract

Lamprophyre dikes and heterolithic breccia zones, some of which are diamondiferous, crosscut 2701 Ma cycle 3 volcanic sequences of the central Michipicoten greenstone belt at Wawa. Available U-Pb geochronology indicates that lamprophyre dikes were emplaced at 2685 to 2674 Ma. Field relationships show that the undated breccia zones predate lamprophyre dikes and are constrained in age between 2701 and 2674 Ma.

The mineralogical and geochemical compositions of the lamprophyre dikes indicate that they are mainly spessartites that have been weakly foliated and metamorphosed. The dikes are up to 5 m in width and typically have a green, medium-grained, granoblastic to decussate groundmass of actinolite, biotite, chlorite, albite, calcite, epidote and titanite. Some samples contain amphibole or biotite macrocrysts, chromite and clinopyroxene. Lamprophyre dikes contain highly rounded mafic to ultramafic xenoliths that are variable in size up to 0.3 m and range in abundance from a few percent to 80% of a dike. The xenoliths are highly altered and composed of Mg-rich actinolite, talc and biotite. Many xenoliths are zoned with a core of coarse-grained radiating actinolite enveloped by a mica-rich reaction rim.

Heterolithic breccia at the Engagement and Cristal occurrences has a fine-grained foliated mafic to ultramafic matrix represented by an assemblage of actinolite+chlorite+albite+epidote +titanite. Macrocrysts of aluminous amphibole (mainly magnesiohornblende) and diopside occur locally. An assortment of angular to subrounded, granule to boulder-sized and matrix- to clast-supported fragments occurs within breccia units. The breccia fragments typically represent nearby country rocks and include mafic to felsic volcanic rocks and a lesser component of felsic plutonic and ultramafic rocks. The heterolithic breccia zones attain a width of up to 70 m and are locally layered due to concentration of fragments within bands. The units have been variously interpreted as intrusive or volcanic breccias.

A sample of an ultramafic xenolith from a lamprophyre dike is chemically comparable to komatiite in terms of $FeOt+TiO_2$-$MgO$-$Al_2O_3$ systematics and has a Mg# of 84. The xenolith is depleted in most trace elements, particularly heavy rare earth elements relative to primitive mantle. The matrix of breccia from the Engagement and Cristal occurrences has 45% $SiO_2$, Mg#s of 78 to 80, low concentrations of alkali elements and is compositionally transitional between komatiite and basaltic komatiite. Trace elements are enriched from 2 (compatible elements) to 40 (incompatible elements) times primitive mantle values. The primitive mantle normalized trace element profiles of breccia matrix are sloped from left to right with troughs corresponding to Nb, Zr, Hf, and Ti. Known lamprophyre dikes have 47 to 48% $SiO_2$, Mg#s of 66 to 69 and are calc-alkalic. In comparison with breccia matrix, lamprophyre dikes are enriched in most trace elements except some transition metals (Co, Cr, Ni). Mantle-normalized trace element profiles of lamprophyre dikes are parallel to and slightly higher than those of breccia matrix. This suggests that the magma representative of the lamprophyres could have fractionated from magma characteristic of the breccia matrix.

The widespread occurrence of the mineral assemblage actinolite+chlorite+epidote is interpreted to indicate that the breccia zones and lamprophyre dikes have been metamorphosed at upper greenschist conditions (temperatures of 375 to 475°C and pressures of 1 to 5 kbars).

Two breccia matrix samples of comparable weight were collected from the Engagement occurrence and processed by magnetic and heavy liquid separation techniques. One sample produced a 0.27 gm heavy mineral concentrate of pyrite, rutile, zircon and titanite with accessory diamond whereas the other sample produced a 0.009 gm heavy mineral concentrate dominated by zircon with no diamonds. The diamond grains include whole, chipped and broken crystals, most of which represent colourless equidimensional octahedra with flat to stepwise lamellar surfaces showing little evidence of resorption. Chemically primitive rocks (higher Mg#, higher transition metals including Cr, Ni and Co and lower REE and LILE) such as the breccia matrix seem to contain more diamonds than evolved lamprophyre dikes although the processing indicates that diamonds are not evenly distributed in the breccia. Further work is required to define the distribution of diamonds within the various host rocks as well as the age, form, distribution and mode of origin of the heterolithic breccias.

# Petrography, Chemistry and Diamond Characteristics of Heterolithic Breccia and Lamprophyre Dikes at Wawa, Ontario

D. Stone[1] and L. Semenyna[2]

Ontario Geological Survey
Open File Report 6134

2004

[1]Geoscientist, Precambrian Geoscience Section, Ontario Geological Survey
Ministry of Northern Development and Mines, Sudbury, Ontario, Canada, P3E 6B5
denver.stone@ndm.gov.on.ca

[2]Scientist, Geoscience Laboratories, Ontario Geological Survey
Ministry of Northern Development and Mines, Sudbury, Ontario, Canada, P3E 6B5
linda.semenyna@ndm.gov.on.ca

# Introduction

In recent years, mineral exploration has led to the discovery of diamonds in Archean lamprophyre dikes and heterolithic breccia zones of the central Michipicoten greenstone belt at Wawa, Ontario. These diamond occurrences are unusual in terms of their host rock characteristics and age compared to most diamond occurrences of Ontario that are associated with kimberlite pipes of Jurassic or Mesoproterozoic age (Sage 1996; 2000a). The lamprophyre dikes and breccia zones represent a potential new source of diamonds but have been largely unstudied until recently.

Research by the Ontario Geological Survey, on the diamond occurrences at Wawa includes the study of the petrography, mineral chemistry and rock chemistry of the diamondiferous "Sandor" dike by Sage (2000b). Vaillancourt, Wilson and Dessureau (2003) have initiated detailed mapping of the diamond-bearing rocks and dominantly volcanic host sequences of the Michipicoten greenstone belt. Ayer et al. (2003) have investigated the timing and petrogenesis of the diamondiferous lamprophyres. The purpose of this study is to briefly describe and compare the petrography, mineral chemistry and rock chemistry of several lamprophyre dikes and breccia zones. The characteristics of diamonds in material representing the matrix of heterolithic breccia are examined. The results of this study are based on sampling of limited outcrop exposures and must be considered preliminary. The current bedrock mapping will provide a basis for new and focused research on the lamprophyre dikes and breccia zones.

# Regional Geology

Presently known diamondiferous lamprophyre dikes and breccias occur within the central Michipicoten greenstone belt near Wawa, Ontario. The Michipicoten greenstone belt (Figure 1a) is a complexly curved and bifurcated enclave of metamorphosed supracrustal rocks intruded and embayed by felsic plutons of the Wawa-Abitibi Subprovince. It extends 140 km east-northeast from the shores of Lake Superior and is composed of an assortment of mafic to felsic volcanic rocks and associated sedimentary rocks.

Based on geologic mapping by R. P. Sage between 1979 and 1994 (see summary report of Sage 1994) and geochronologic studies by A. Turek (e.g. Turek, Sage and Van Schmus 1992), the Michipicoten greenstone belt has been subdivided into 3 supracrustal cycles with ages of 2.9, 2.75 and 2.70 Ga (Figure 1b). All Archean supracrustal rocks are metamorphosed however the prefix meta- is not applied to rock names used in this report for sake of brevity. Rocks comprising the oldest cycle (cycle 1) occur at the south margin of the Michipicoten greenstone belt and attain a width of up to 4 km. The basal part of cycle 1 is made up of massive to pillowed komatiitic flows intruded by mafic sills. The ultramafic rocks are overlain by intermediate to felsic tuffs and breccias capped by thinly bedded chert-magnetite-sulphide iron formation. An intermediate tuff from cycle 1 has a U-Pb zircon age of 2889±9 Ma (Turek, Sage and Van Schmus 1992).

Volcanic rocks of cycle 2 comprise pillowed and massive mafic flows overlain by intermediate to felsic tuffs and breccias. These directly overlie cycle 1 and otherwise occur somewhat sporadically through western and central parts of the Michipicoten greenstone belt. Felsic volcanic flows and tuffs from cycle 2 are dated at 2746±11, 2741±5 and 2729±3 Ma (Turek, Sage and Van Schmus 1992). The volcanic rocks of cycle 2 are capped by a 100 m-thick unit of thin bedded to massive iron formation. The iron formation was mined extensively in the Wawa area.

A)

LEGEND

B)

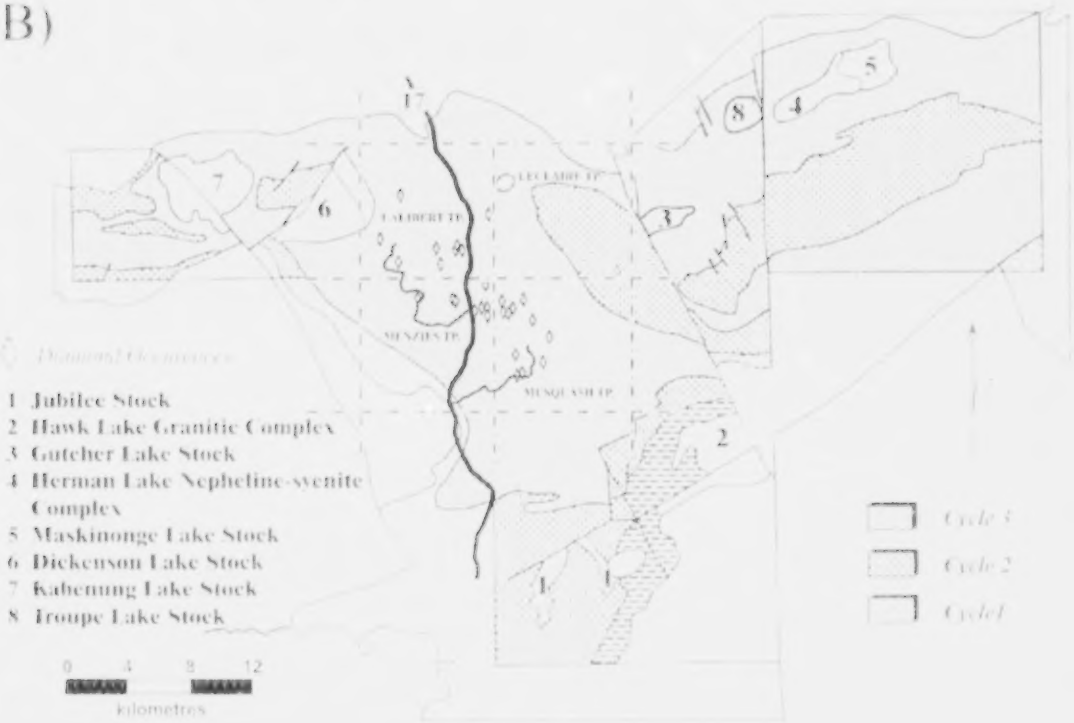
1 Jubilee Stock
2 Hawk Lake Granitic Complex
3 Gutcher Lake Stock
4 Herman Lake Nepheline-syenite Complex
5 Maskinonge Lake Stock
6 Dickenson Lake Stock
7 Kabenung Lake Stock
8 Troupe Lake Stock
0 4 8 12
kilometres
Cycle 3
Cycle 2
Cycle 1

A)

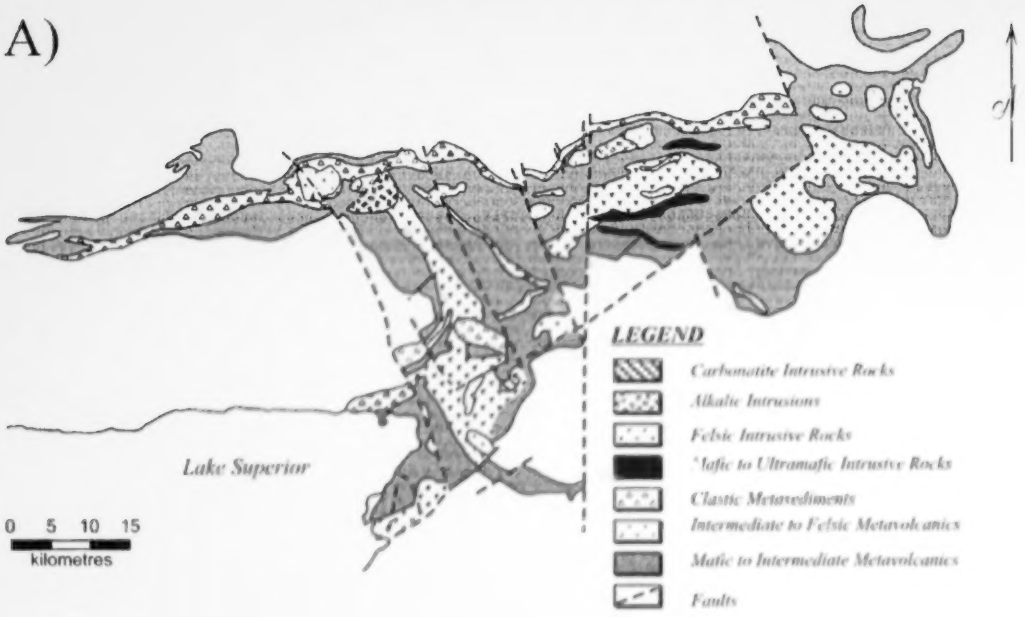
LEGEND
Carbonatite Intrusive Rocks
Alkalic Intrusions
Felsic Intrusive Rocks
Mafic to Ultramafic Intrusive Rocks
Clastic Metasediments
Intermediate to Felsic Metavolcanics
Mafic to Intermediate Metavolcanics
Faults
Lake Superior
0 5 10 15
kilometres

B)

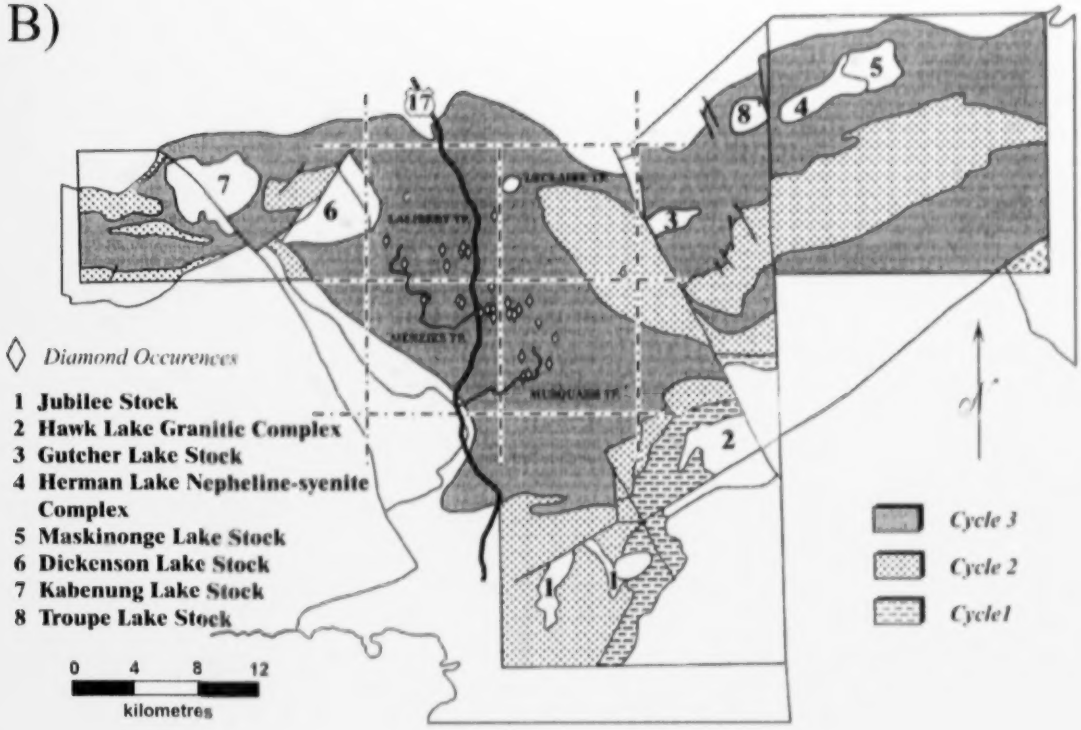
Diamond Occurences
1 Jubilee Stock
2 Hawk Lake Granitic Complex
3 Gutcher Lake Stock
4 Herman Lake Nepheline-syenite Complex
5 Maskinonge Lake Stock
6 Dickenson Lake Stock
7 Kabenung Lake Stock
8 Troupe Lake Stock
Cycle 3
Cycle 2
Cycle1
0 4 8 12
kilometres

C)

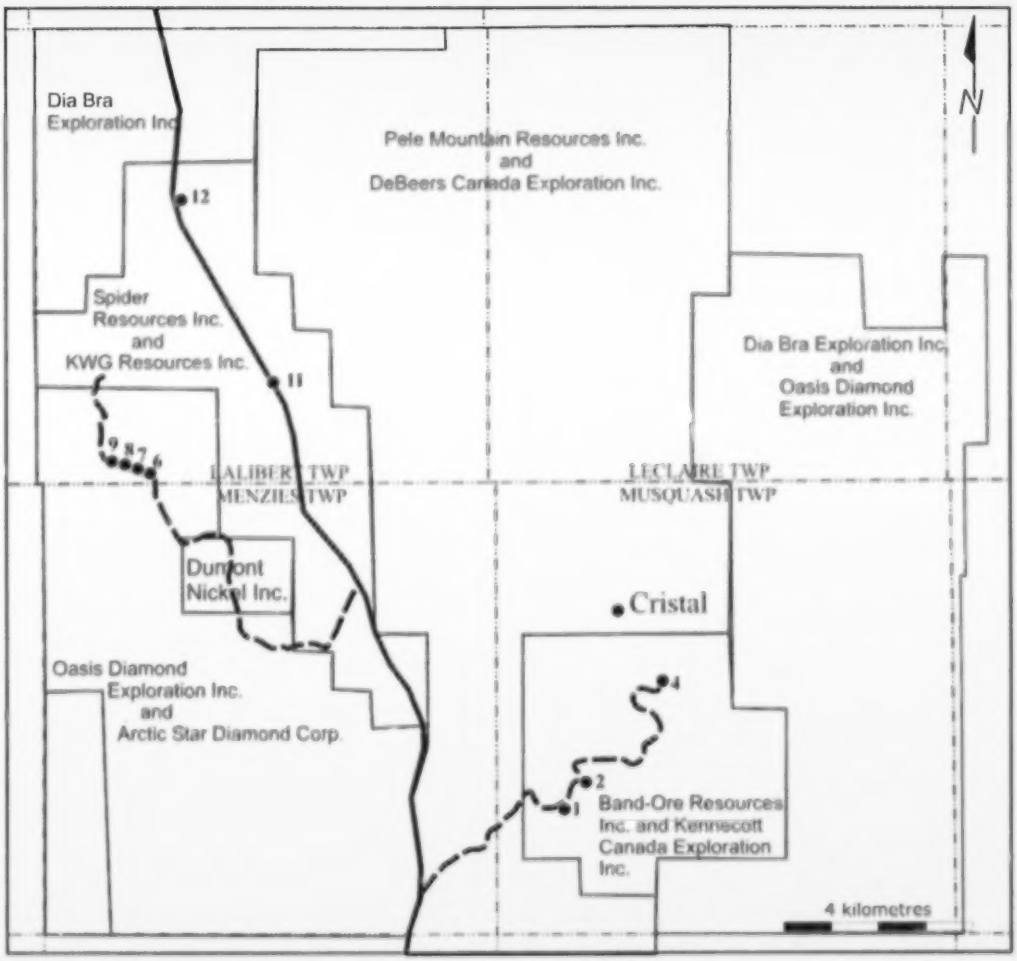


1. Stop 1A GQ
2. Stop 2 Barnet Lake Zone
4. Stop 4 Engagement Occurrence
6. Stop 6 Lamprophyre Dike*
7. Stop 7 Heterolithic Breccia*
8. Stop 8 Giant Inclusion Breccia*
9. Stop 9 Heterolithic Breccia*
11. Stop 11 Sandor Dike
12. Stop 12 Xenolithic Dike

* Oasis Occurrence

**Figure 1**: (a) Geology of the Michipicoten greenstone belt, from Sage (1994); (b) distribution of volcanic cycles, internal plutons and diamond occurrences in the central Michipicoten greenstone belt from Sage (1994) and Vaillancourt, Wilson and Dessureau (2003); (c) sample locations for this study (numbers refer to stops listed in Table 1).

Volcanic rocks of cycle 3 occur in central and northern parts of the Michipicoten greenstone belt. Cycle 3 is marked by a basal sequence of pillowed and massive tholeiitic mafic volcanic flows overlying the iron formation of cycle 2. The mafic sequences attain a thickness of 1 km and are overlain by intermediate to felsic tuffs and polymictic to oligomictic breccias. Quartz+feldspar crystal tuff and an intermediate tuff from cycle 3 have U-Pb zircon ages of 2701±8 Ma (Turek, Sage and Van Schmus 1992) and 2701.4±2.1 Ma (Ayer et al. 2003). The intermediate to felsic tuffs are associated with clastic sedimentary sequences including cross-bedded sandstone and tonalite cobble conglomerate (Doré conglomerate). Corfu and Sage (1987; 1992) reported an age of 2698±2 Ma for a tonalite clast in the Doré conglomerate and maximum ages of 2680±3 and 2682±3 for sedimentary sequences in northern and central parts of the Michipicoten greenstone belt. The geochronology and structural evidence indicates that sedimentation continued after cycle 3 volcanism and predated a major folding and faulting event. Arias and Helmstaedt (1990) noted that strata comprising cycle 3 in the central Michipicoten greenstone belt is upside down and represents the overturned limb of a belt-scale recumbent nappe fold. The inverted limb of the nappe fold is refolded and imbricated by south-verging thrust faults, which cause local repetitions of the stratigraphic sequence.

Felsic plutonism occurred synchronous with the major volcanic cycles and continued after volcanism at Wawa. The Murray-Algoma porphyry and Regnery biotite granite of the Hawk Lake granitic complex at the south margin of the Michipicoten greenstone belt (*see* Figure 1b) are dated at 2881±6 and 2888±2 Ma, respectively (Turek, Sage and Van Schmus 1992; Turek, Smith and Van Schmus 1984). These plutonic rocks were intruded synchronous with volcanism of cycle 1. The Jubilee granitic stock (*see* Figure 1b) was dated by Sullivan, Sage and Card (1985) at 2745±3 Ma and is coeval with cycle 2 volcanism. Compositionally variable intrusions ranging from tonalite through granodiorite to granite are situated south and west of the Michipicoten greenstone belt and have ages ranging from 2698 to 2693 Ma (Turek, Keller and Van Schmus 1990; Turek Smith and Van Schmus 1984). These intrusions were emplaced a few million years after the peak of volcanic activity associated with cycle 3.

In summarizing U-Pb zircon ages Turek, Sage and Van Schmus (1992) noted that the majority of felsic plutonic rocks in the area of the Michipicoten and neighbouring greenstone belts were emplaced from 2686 to 2662 Ma and significantly post-date the youngest cycle of volcanism at 2701 Ma. These authors correlated the post-volcanic plutonic event with the Kenoran Orogeny in the Wawa area. Among intrusions emplaced during the late plutonic event is the syenitic Dickenson Lake stock (*see* Figure 1b), which has an age of 2677±5 Ma (Turek, Sage and Van Schmus 1992).

Foliated lamprophyre dikes and heterolithic breccia zones are concentrated in Lalibert, Menzies, Leclaire and Musquash townships about 20 km north of Wawa (*see* Figures 1b,c and discussion below). Sage (2000b) reported an age of 2703±42 Ma on titanite from the matrix of the Sandor dike of the foliated lamprophyre suite. Subsequent dating of a gneissic xenolith from the Sandor dike yielded an age of 2684.9±1.4 Ma (Ketchum, Kamo and Davis 2003). The latter constrains the maximum emplacement age of the Sandor dike at 2685 Ma. Stott et al. (2002) quoting unpublished data of R. P. Sage reported a titanite age of 2674±8 Ma for a lamprophyre dike at the GQ property. A lamprophyre dike from the Enigma property in Lalibert Township yielded a variety of zircon grains ranging in age from 2685 to 2715 Ma (Ketchum, Kamo and Davis 2003). The older zircon grains are interpreted as xenocrysts whereas the youngest population of zircon grains may be either xenocrystic or magmatic (Ayer et al. 2003). Accordingly, the 3 youngest zircon grains, with an average age of 2685.0±1 Ma, may represent a maximum age of dike emplacement (xenocrysts) or the absolute age of dike emplacement (magmatic). Stott et al. (2002) postulated a coeval and possibly comagmatic association between diamondiferous lamprophyre dikes and breccias and late quartz-undersaturated intrusions such as the Dickenson Lake stock in the Michipicoten greenstone belt.

The Michipicoten greenstone belt is intruded by diabase dikes and unfoliated lamprophyre dikes. Sage (1994) noted variable alteration and fabric development within diabase dikes and suggested that there may be Archean and Proterozoic varieties. The unfoliated lamprophyre dikes include the xenolithic Nicholson ultramafic dike located on the Magpie River, 10 km southwest of Wawa. This dike has a Rb-Sr phlogopite age of 1100±40 Ma (Sage and Crabtree 1997) and a U-Pb perovskite age of 1123±13 Ma (R. Sage, personal communication, 2004). The dike appears to have been emplaced at a time broadly coeval with the onset of Midcontinent Rift volcanism at 1109 Ma. Undeformed lamprophyre dikes occur at the southeast margin of the Michipicoten greenstone belt and are geographically separated from the foliated lamprophyre dikes. Queen et al. (1996) obtained a U-Pb perovskite age of 1143±12 Ma for a lamprophyre dike at Wawa and noted a similarity in age between this dike and dikes of the Kapuskasing Structural Zone and the Abitibi dike swarm.

# Foliated Lamprophyre Dikes and Heterolithic Breccias: Outcrop Characteristics

Although diamonds were initially discovered in alluvium (Morris, Murray and Crabtree 1994), two principal bedrock sources of diamonds have subsequently been recognized in the Wawa area (*see* locations in Figure 1b). These include lamprophyre dikes and zones of heterolithic breccia, although in many instances it is difficult to distinguish one from the other. This problem arises because the lamprophyre dikes contain variable proportions of assorted enclaves[1] and enclave-laden dikes can have the appearance of breccia material.

Lamprophyre dikes intrude cycle 3 volcanic rocks of the Michipicoten greenstone belt. Lefebvre et al. (2003) noted that lamprophyre dikes also intrude heterolithic breccias at many localities. The age-relation of heterolithic breccias to cycle 3 volcanic rocks is less well understood because it is unclear whether the breccias are intrusive or extrusive in origin. Sage (1994) included heterolithic breccias as a type of lamprophyre dike and Stott et al. (2002) cited intrusive contacts and abundant volcanic xenoliths as evidence that the heterolithic breccias originated as diatreme-like breccia dikes and post-date cycle 3 volcanic rocks. In contrast, Wilson (2002) and Lefebvre et al. (2003) interpreted the heterolithic material as originating from volcanic tuff eruptions and volcaniclastic debris-flows associated with cycle 3 volcanism.

For purposes of description, the classification of Wawa lamprophyres by Sage (1994) is adopted in this study. Sage (1994) identified three types of lamprophyric material including:

- dikes composed mostly of biotite;
- dikes composed of a biotite and actinolite matrix with large rounded xenoliths (up to 0.3 m in size) composed of actinolite and talc;
- heterolithic breccias.

Biotite-rich dikes are fine-grained and typically less than 1 m wide. They have not been extensively described and were not encountered in this study. Xenolithic dikes, such as the Sandor dike (Sage 2000b), attain a width of up to 5 m although 100 m wide dikes are reported (Ann Wilson, personal communication, 2004). There is little recorded information on the orientations of the dikes. The dike

[1] Summary of terminology for inclusions in lamprophyres (Rock 1991)

| | Accidental | Cognate | Unknown (non-genetic term) |
|---|---|---|---|
| Crystals | Xenocryst | Phenocryst | Macrocryst (megacryst if >5 mm) |
| Rocks | Xenolith | Autolith | Enclave |

matrix is fine-grained, dark green and weathers brown. The matrix is represented by an assemblage of minerals including some or all of actinolite, biotite, chlorite, titanite, albite, calcite and magnetite. Macrocrysts (up to 1 mm in size) of actinolite and biotite are common.

Xenoliths within the lamprophyre dikes are commonly ultramafic compared to the matrix and probably represent accidental rather than cognate inclusions. These xenoliths are highly rounded, variable in size up to 0.3 m and range in abundance from a few percent to 80% of the dike. The xenoliths are highly altered and are composed of magnesium-rich actinolite, talc and biotite. Many xenoliths are zoned with a core of coarse-grained radiating actinolite enveloped by a mica-rich reaction rim. The Sandor dike contains rare examples of gneissic xenoliths (Sage 2000b; Ayer et al. 2003).

Heterolithic breccias form thick (up to 70 m) units distributed broadly through Lalibert, Menzies, Leclaire and Musquash townships. Walker (2003) noted that breccia zones are concentrated within three northwest-trending zones. The matrix of the breccia units consists of an assemblage of minerals similar to that found in xenolithic dikes although mafic minerals predominate over felsic minerals in the breccia matrix. An assortment of angular to subrounded, granule to boulder-sized and matrix- to clast-supported fragments occurs within breccia units. The breccia fragments represent a wide variety of lithologies including mafic to felsic volcanic rocks and a lesser component of felsic plutonic and ultramafic rocks. Some fragments have aphanitic rinds and have been interpreted as lapilli (Lefebvre et al. 2003). Large blocks of mafic, pillowed volcanic country rocks occur within the breccia unit at the Cristal occurrence (*see* Figure 1c).

The breccia units contain one or two foliations defined by alignment of actinolite grains (Lefebvre et al. 2003); fragments are locally stretched and aligned with the foliation. The breccia units can be layered due to the concentration of fragments. The layering is typically developed on a scale of several metres and has been variously attributed to concentration of fragments due to flow of a fragment-laden magma through a dike (Stott et al. 2002) or volcanic eruption (Lefebvre et al. 2003).

Recent bedrock mapping by Vaillancourt et al. (2003) identified extensive intrusion breccia characterized by a variety of mela- to leucogabbro and gneissic fragments within a dioritic matrix in southwest Menzies Township. These authors suggest that the intrusion breccia developed at the margin of the batholithic complex, southwest of the Michipicoten greenstone belt, and is unrelated to the heterolithic breccias discussed above.

# Petrography

Fourteen samples (02DS86 to 02DS99; Table 1) of lamprophyre dikes and breccia zones were collected for petrographic and chemical analysis. The samples were derived from locations shown in Figure 1c and correspond to the field trip stops of Wilson (2002) as listed in Table 1. The breccia samples can be further subdivided according to whether they represent breccia matrix or a combination of matrix and fragments. Sample 02DS92 represents an actinolitic xenolith in a lamprophyre dike and 02DS97 is from a late diabase dike.

Thin sections of the samples were examined using an Olympus BH-2 microscope and brief petrographic descriptions of various groups of samples are provided below.

**Table 1:** Sample description and disposition.

| Sample No. | Area | Field Rock Description (Rock Type Code) | Stop No.* (Wilson 2002) | UTM east** | UTM north** | Sample Description | Polished Section | Mineral Chemistry | Rock Chemistry | Diamond Extraction |
|---|---|---|---|---|---|---|---|---|---|---|
| 02DS86 | Engagement occurrence | breccia matrix (1) | Stop 4 | 667729 | 5336050 | Fine-grained, medium green, well foliated actinolite schist with 20% macrocrysts (up to 1mm) of dark hornblende and light actinolite. Representative of the breccia matrix. | yes | yes | yes | yes |
| 02DS87 | Engagement occurrence | breccia matrix (1) | Stop 4 | 667729 | 5336050 | Fine-grained, medium to light green, weakly foliated actinolite schist with 20% macrocrysts (up to 1 mm) of dark hornblende and light actinolite. Contains 5% angular fragments of fine-grained micaceous material (up to 20 mm). Representative of the breccia matrix. | yes | yes | yes | yes |
| 02DS88 | Engagement occurrence | breccia (2) | Stop 4 | 667729 | 5336050 | A breccia with a matrix like 02DS86 and 50% subrounded fragments up to 25 mm. The fragments include fine-grained dark material, fine grained felsic material, medium-grained micaceous mafic material and tonalite. | yes | yes | yes | |
| 02DS89 | Cristal occurrence | breccia matrix (1) | N/A | 666482 | 5337338 | Fine-grained, pale green, weakly foliated, soft actinolitic rock with 20% macrocrysts (up to 1 mm) of amphibole. Contains 5% rounded fragments of medium-grained felsic material. Representative of breccia matrix. | yes | yes | yes | |
| 02DS90 | Cristal occurrence | breccia (2) | N/A | 666482 | 5337338 | A breccia with a matrix like 02DS89 and 80% subangular fragments up to 60 mm. Fragments include medium-grained dark micaceous material and a variety of fine-grained mafic to felsic and probably volcanic clasts. | yes | yes | yes | |
| 02DS91 | GQ Diamond Discovery Site | altered lamprophyre dike with banded mafic xenoliths (3) | Stop 1A | 665570 | 5333068 | Medium-grained, dark green, weakly foliated micaceous rock with 20% mica macrocrysts to 3 mm. Contains a large rounded, weakly gneissic mafic xenolith. | yes | yes | yes | |
| 02DS92 | Barnet Lake Zone (xenolith) | actinolitic xenolith in a mafic dike (4) | Stop 2 | 665425 | 5334525 | Round xenolith (100 mm diameter) of coarse-grained tremolite and calcite in a dark fine-grained matrix. | yes | yes | yes | |
| 02DS93 | Lamprophyre Dike (Arctic Star) | lamprophyre dike with mafic inclusions | Stop 6 | 657140 | 5340023 | Medium-grained, dark green, weakly foliated micaceous rock with 20% macrocrysts (up to 2 mm) of mica and carbonate. Contains 15% rounded coarse-grained enclaves compositionally similar to the matrix. | yes | yes | | |
| 02DS94 | Heterolithic Breccia | lamprophyre matrix with heterolithic fragments (2 or 3) | Stop 7 | 656724 | 5340156 | Medium-grained, black, weakly foliated micaceous rock with diffuse micaceous megacrysts to 5 mm. Representative of breccia matrix. | yes | yes | yes | |
| 02DS95 | Giant Inclusion Breccia | breccia matrix with heterolithic fragments (2 or 3) | Stop 8 | 656440 | 5340375 | Fine-grained, dark green, well foliated amphibole schist with 25% stretched xenoliths of coarse-grained mafic and felsic plutonic material. | yes | yes | | |
| 02DS96 | Diamondiferous Heterolithic Breccia | breccia matrix (1 or 3) | Stop 9 | 656022 | 5340393 | Fine-grained, black weathering brown, weakly foliated micaceous rock with 30% aggregates of dark mica and light carbonate to 3 mm. Representative of the breccia matrix. | yes | yes | yes | |
| 02DS97 | Fine grained dike | fine-grained diabase dike (5) | Stop 9 | 656022 | 5340393 | Fine-grained, black weathering brown, massive rock with possible diabase texture. From a 0.2 m-wide dike in breccia. | yes | yes | yes | |
| 02DS98 | "Sandor" dike | fine-grained spessartite lamprophyre with meta-pyroxenite xenoliths (3) | Stop 11 | 659967 | 5342068 | Medium-grained, dark green to black, weakly foliated rock with 5% black amphibole macrocrysts to 3 mm. Contains 20% large rounded xenoliths of medium- to coarse-grained mafic to ultramafic material. | yes | | yes | |
| 02DS99 | Non-diamondiferous mantle xenolith-rich dike | spessartite lamprophyre dike with round actinolitic xenoliths (3) | Stop 12 | 657250 | 5346800 | Coarse-grained, dark green to brownish black massive rock with mica and amphibole macrocrysts to 3 mm and diffuse black xenoliths. | yes | | yes | |

* Stops refer to the field trip stops of Wilson (2002).
** UTM Coordinates are in NAD 27, Zone 16.

## LAMPROPHYRE DIKES

Samples 02DS91, 02DS93, 02DS98 and 02DS99 are derived from material, interpreted on the basis of field relations, as representing lamprophyre dikes. The samples are characterized by a green, medium-grained, granoblastic to decussate groundmass of actinolite, biotite, chlorite, plagioclase and accessory minerals. Some samples contain amphibole or biotite macrocrysts up to 1 mm in size. Sample 02DS99 is somewhat coarser grained and shows acicular actinolite macrocrysts up to 3 mm in size (Figure 2). Although some macrocrysts have possibly originated as accidental inclusions, the majority appears on the basis of their compositional similarity to groundmass minerals to have grown as cognate phenocrysts or during metamorphism.

Sample 02DS93 is somewhat more ultramafic than other lamprophyres due to a scarcity of feldspar and is characterized by irregular coarse patches of actinolite and biotite. A pleochroic amphibole of hornblende composition occurs locally. Samples 02DS91 and 02DS98 contain ultramafic enclaves of probable accidental origin. The xenolith in 02DS91 is a strongly foliated to banded aggregate of actinolite and chlorite whereas that in 02DS98 is oval and zoned with a tremolite+calcite core and biotite-rich rim.

Table 2 provides a summary of mineral assemblages. Aluminum-depleted, calcic amphibole (magnesium-rich actinolite) occurs widely in lamprophyre dikes. This, combined with albitic plagioclase, chlorite and calcite and severely altered ultramafic xenoliths, imply pervasive metamorphism or alteration of the dikes.

## BRECCIA MATRIX

Samples 02DS86, 02DS87, 02DS89 and 02DS96 represent the matrix of breccia zones at the Engagement, Cristal and Oasis occurrences. The matrix material at the Engagement and Cristal occurrences is typically fine-grained, green, weakly foliated actinolite schist. Approximately 20% macrocrysts of actinolite (up to 1.0 mm) occur throughout the matrix and appear as diffuse light aggregates in Figure 3. Although albite occurs in all samples, it is less abundant (<10%) than in lamprophyre dikes and implies a somewhat more ultramafic composition for the breccia matrix than for the lamprophyre dikes. Titanite is fairly abundant (up to 8%) and calcite, epidote, apatite and sulphide minerals occur locally. The opaque minerals in breccia samples have not been investigated extensively and may include magnetite and chromite. These spinel group minerals have been identified in lamprophyre dikes of the area (Sage 2000b; Williams 2002).

In addition to the small, light actinolite macrocrysts of probably metamorphic origin, the breccia matrix also contains rare dark macrocrysts of variably acicular to oval shape and range up to 2 mm in size (*see* Figure 3). The dark macrocrysts are composed of a pleochroic amphibole. The largest amphibole grain contains oval inclusions of clinopyroxene and rims of the dark amphibole grains are converted to actinolite. The dark macrocrysts may represent accidental or cognate crystals and in either case appear to have developed prior to metamorphism with subsequent partial conversion to actinolite.

Sample 02DS96 from the Oasis occurrence is more felsic and mineralogically distinct from other samples of breccia matrix. Biotite comprises approximately 50% of the rock with the remainder made up of albite, calcite and ankerite with accessory magnetite, apatite and quartz. Calcite occurs in the matrix and as macrocrysts.

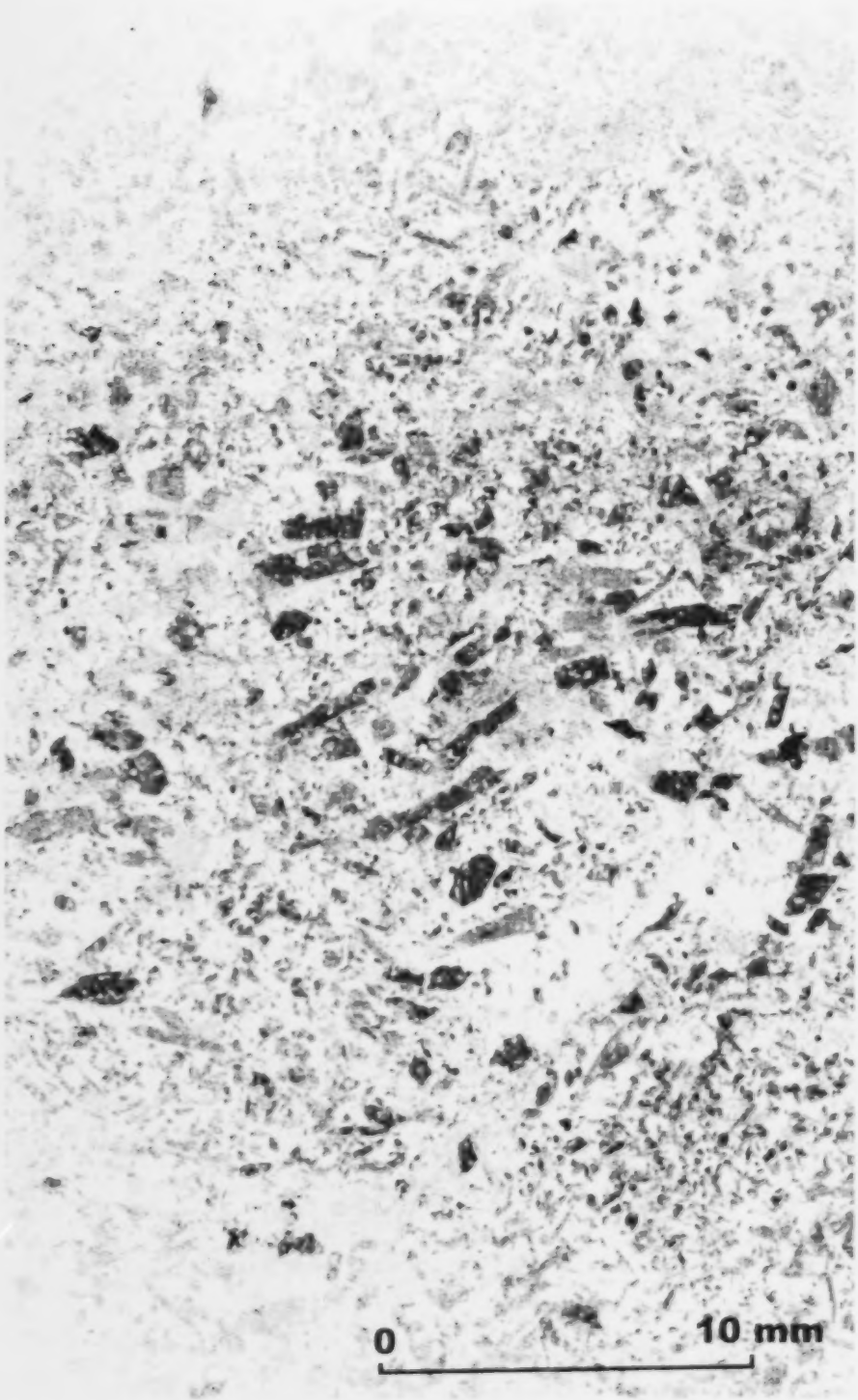


**Figure 2**: Scanned image of a thin section of the matrix of a lamprophyre dike. Sample 02DS99, Stop 12.

Mineral assemblages of the breccia matrix samples are summarized in Table 2, and with the exception of 02DS96, are dominated by actinolite+chlorite+albite similar to the lamprophyre dikes. On the basis of limited samples, the dark amphibole macrocrysts at the Engagement and Cristal occurrences appear to be the main mineralogical distinction between the matrices of heterolithic breccias and lamprophyre dikes.

**Table 2:** Mineral assemblages.

| Sample No. | Rock Type (Rock Type Code) | Mineral Assemblage | Analyzed Minerals |
|---|---|---|---|
| 02DS91 | Lamprophyre dike (3) | Actinolite+biotite+albite+chlorite+titanite+apatite | Actinolite, albite, mica, chlorite |
| 02DS93 | Lamprophyre dike (3) | Hornblende+actinolite+biotite+chlorite+magnetite +pyrite+apatite+clear unknown | Chlorite |
| 02DS98 | Lamprophyre dike (3) | Amphibole+biotite+plagioclase+calcite+titanite | |
| 02DS99 | Lamprophyre dike (3) | Amphibole+biotite+plagioclase+calcite+titanite | |
| 02DS86 | Breccia matrix (1) | Actinolite+magnesiohornblende (phenocryst)+calcite +chlorite+albite+titanite+apatite+chalcopyrite | Magnesiohornblende, actinolite, chlorite, albite |
| 02DS87 | Breccia matrix (1) | Actinolite+magnesiohastingsite (phenocryst)+albite +chlorite+calcite+epidote+titanite+opaque | Magnesiohastingsite, actinolite, albite, chlorite |
| 02DS89 | Breccia matrix (1) | Tschermakite+clinopyroxene (phenocryst) +actinolite+albite+chlorite+titanite+unknown white | Clinopyroxene, tschermakite, actinolite, albite, chlorite |
| 02DS96 | Breccia matrix (1 or 3) | Albite+calcite+biotite+ankerite+quartz+apatite +magnetite/hematite | Mica, albite |
| 02DS88 | Breccia (2) | Hornblende+actinolite+albite+biotite+calcite+quartz +epidote+titanite+chalcopyrite | Magnesiohornblende, actinolite, albite, mica, chlorite |
| 02DS90 | Breccia (2) | Magnesiohornblende+actinolite+albite+biotite +titanite+calcite+epidote+chalcopyrite | Magnesiohornblende, albite, mica |
| 02DS94 | Breccia (2 or 3) | Magnesiohornblende+actinolite+biotite+albite +quartz+titanite+apatite+rutile | Magnesiohornblende, actinolite, albite, mica |
| 02DS95 | Breccia (2 or 3) | Magnesiohornblende+actinolite+biotite+chlorite +albite+epidote+calcite+quartz+magnetite/hematite +ilmenite/titanite | Magnesiohornblende, mica, chlorite |
| 02DS92 | Ultramafic xenolith (4) | Tremolite+biotite+calcite | |
| 02DS97 | Diabase dike (5) | Clinopyroxene+amphibole+labradorite+albite+calcite+quartz +ilmenite | Augite, labradorite |

Rock Type Codes: 1-breccia matrix; 2-breccia; 3-lamprophyre dike; 4-ultramafic xenolith; 5-diabase dike.

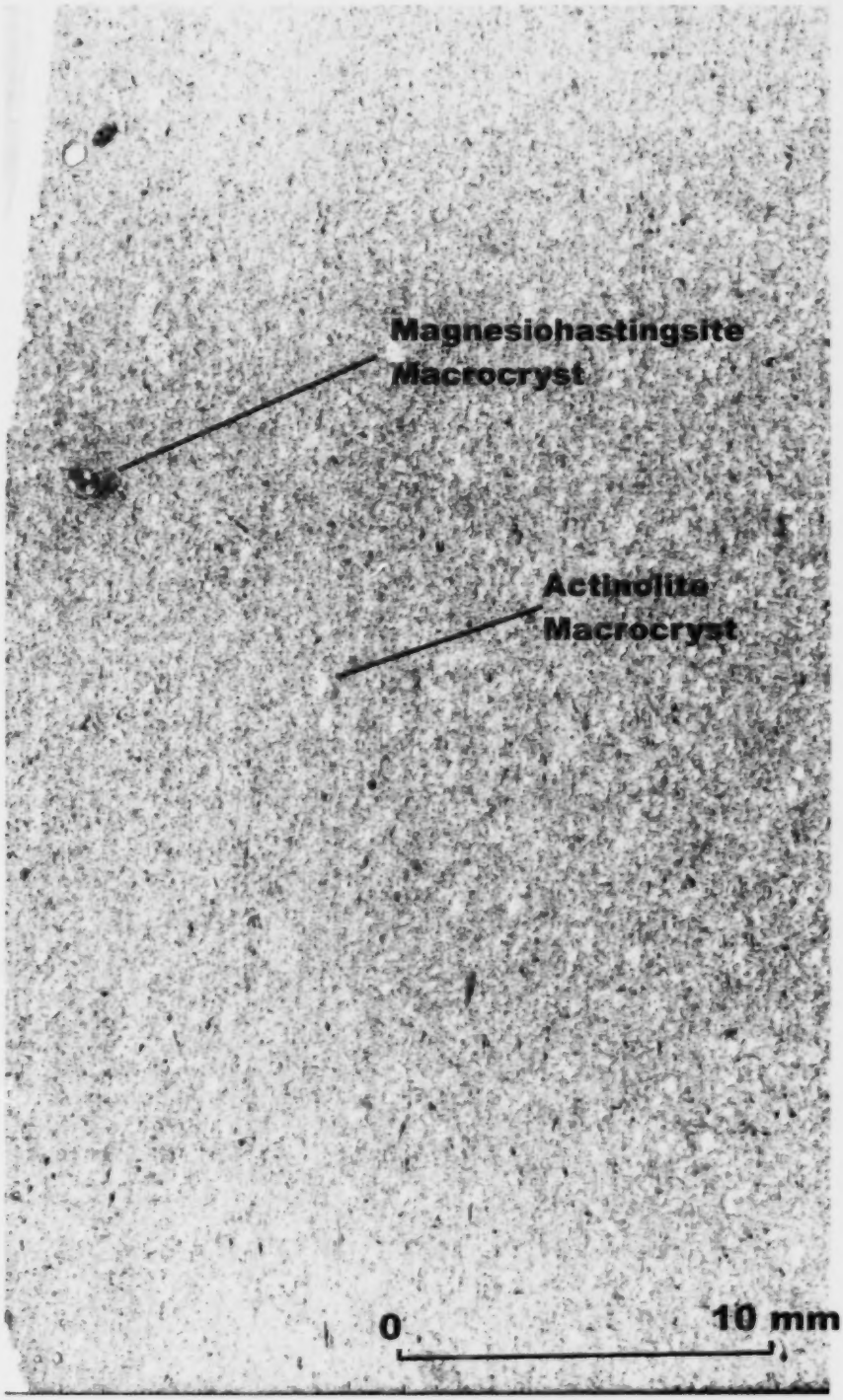


**Figure 3**: Scanned image of a thin section of the matrix of heterolithic breccia. Sample 02DS86, Stop 4.

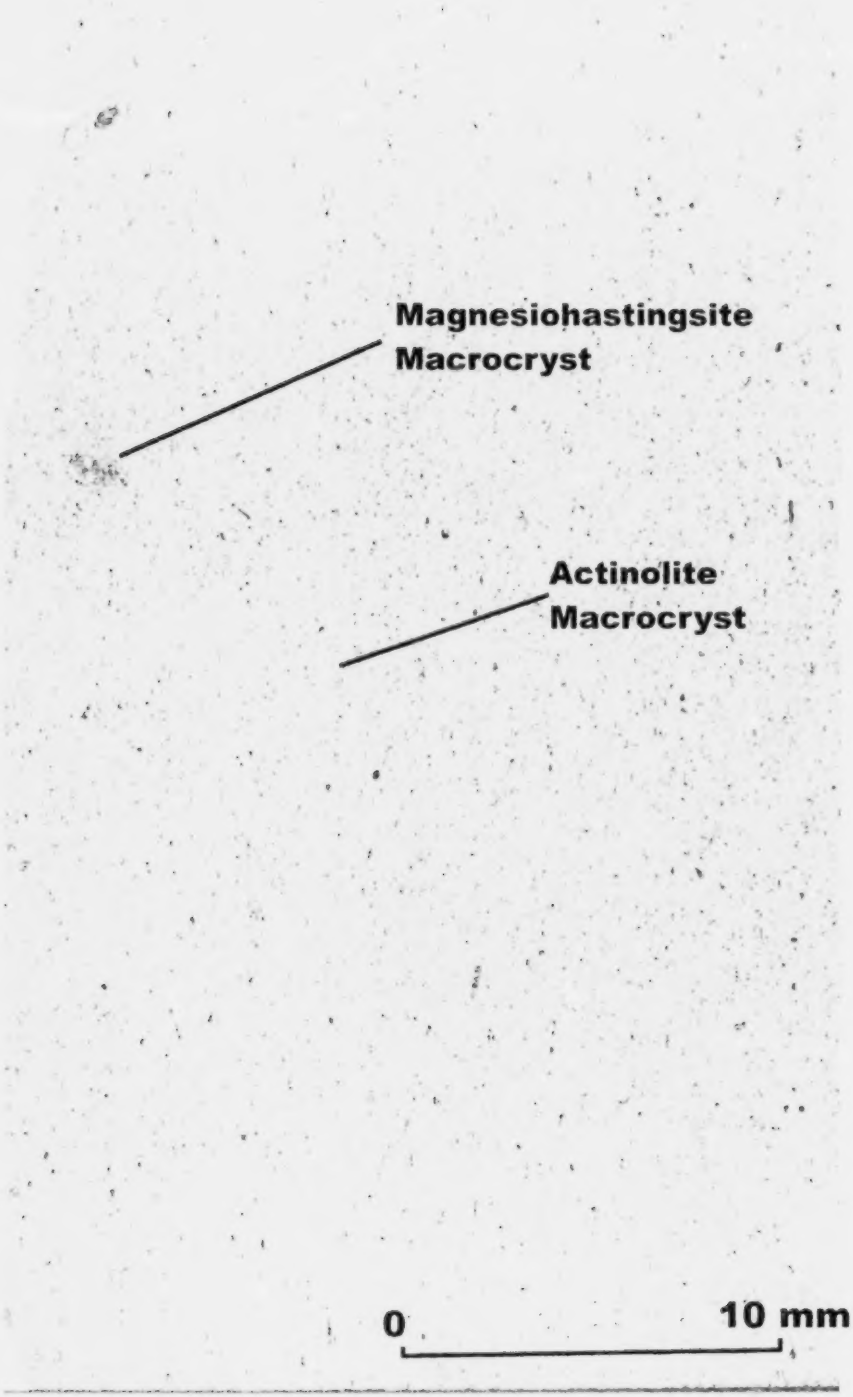


**Figure 3**: Scanned image of a thin section of the matrix of heterolithic breccia. Sample 02DS86, Stop 4.

## HETEROLITHIC BRECCIA

Samples 02DS88, 02DS90, 02DS94, and 02DS95 represent heterolithic breccia containing a variety of fragments within a mafic to ultramafic matrix. Breccia samples are texturally and compositionally variable. Samples 02DS88 and 02DS90 represent breccia from the Engagement and Cristal occurrences (*see* 02DS90 in Figure 4) and have a fine-grained dark matrix. The breccias at these localities show a close-packed assortment of angular and variably mafic to felsic and fine- to coarse-grained clasts that appear to represent altered volcanic material representative of nearby cycle 3 volcanic sequences. The matrix of samples 02DS94 and 02DS95 from the Oasis occurrence (Stop 8 of Wilson 2002) is coarser grained and more felsic with a higher biotite/amphibole proportion than the matrix from breccia at the Engagement and Cristal occurrences. Samples 02DS94 and 02DS95 have a high matix/clast ratio and a granoblastic to decussate texture similar to lamprophyre dikes. Diffuse felsic to intermediate clasts, possibly representative of the nearby volcanic sequences, are embedded in the matrix of samples from the Oasis occurrence.

Mineral proportions of breccia samples fall into two groups (Table 2). Samples from the Cristal and Engagement occurrences (02DS88 and 02DS90) are dominated by actinolite+albite+calcite with rare hornblende. Biotite and quartz occur locally in felsic fragments and the breccias are cut by fractures filled with calcite, epidote and chalcopyrite. In contrast, samples from the Oasis occurrences (02DS94 and 02DS95) are more felsic with a higher proportion of albite and locally calcite and quartz as well as higher biotite/amphibole ratio.

## ULTRAMAFIC XENOLITH

Sample 02DS92 was collected from the central part of an oval ultramafic xenolith in a mafic dike at the Barnett Lake zone. The sample is dominated by a coarse, radiating to decussate, clear to pale green amphibole of tremolitic to magnesium-rich actinolite composition. Carbonate occurs locally and biotite is concentrated at the rims of the xenolith.

## DIABASE DIKE

Sample 02DS97 was collected from a 0.1 m wide dike at the Oasis occurrence. The sample is characterized by fine-grained, dark, massive diabase with 40% labradorite laths set in augite and ilmenite. The augite is partly altered to amphibole and albite occurs as rims on labradorite grains. Quartz and calcite occur locally. The diabase dike appears to represent either the late Archean or Proterozoic diabase dikes recognized by Sage (1994) although the age of this dike is unknown.

# Mineral Chemistry

Mineral compositions were determined using the Cameca microprobe at the Geoscience Laboratories in Sudbury and are listed in Tables 3 to 7. The analyses presented here do not represent the full range of minerals within lamprophyres and breccias but are intended to characterize the dominant mineral species within these rocks. Other minerals can be present. For example, Sage (2000b) reported analyses of chromite and ilmenite grains obtained from heavy mineral concentrates of bulk samples of the Sandor dike. In general, the dominant indicator minerals of kimberlitic rocks including pyrope, olivine, diopside, chromite and ilmenite are rare or absent in lamprophyres and breccias of the Wawa area.

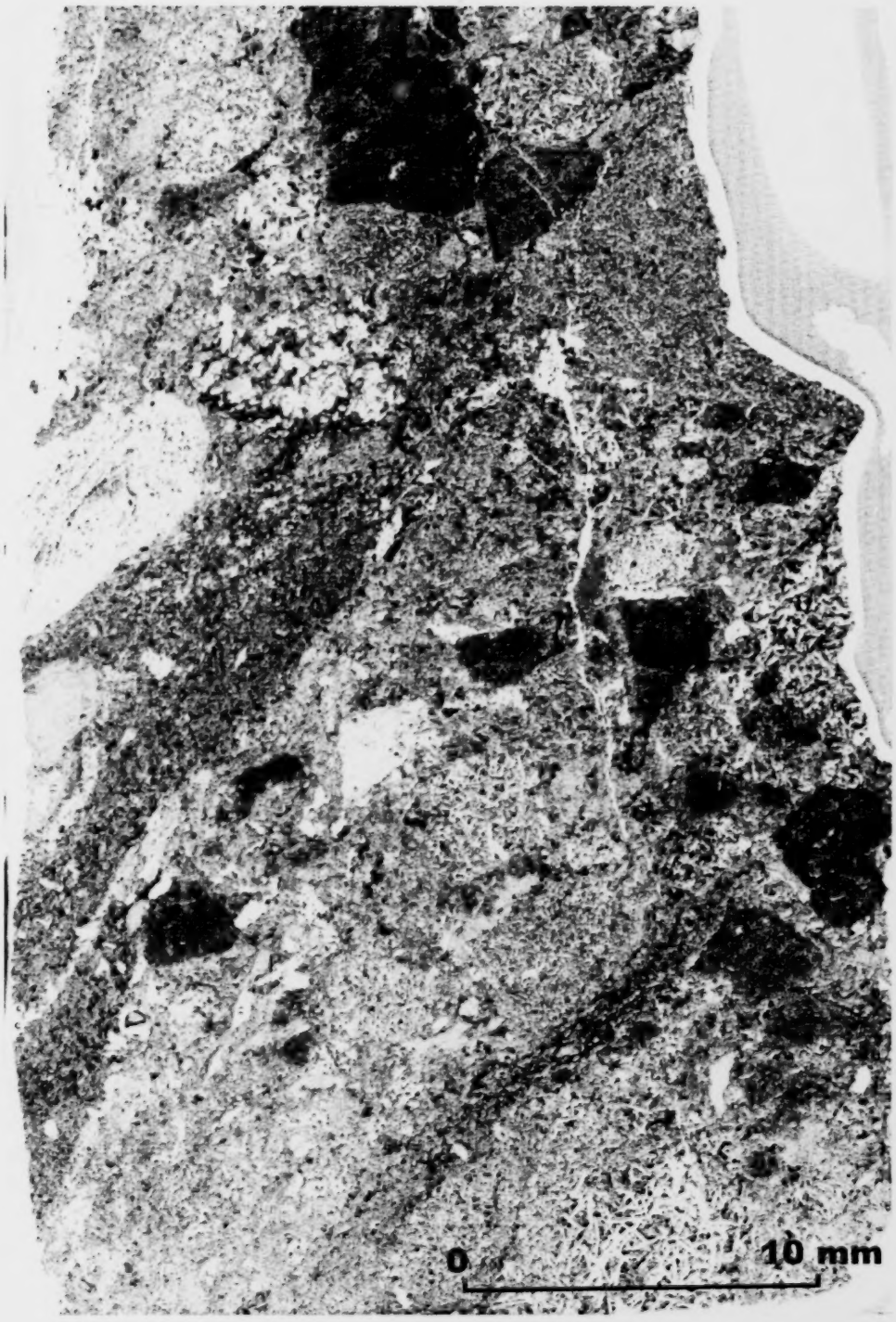


**Figure 4**: Scanned image of a thin section of heterolithic breccia. Sample 02DS90, Cristal occurrence.

**Table 3:** Feldspar analyses.

| Sample | 02DS86 | 02DS87 | 02DS88 | 02DS89 | 02DS90 | 02DS91 | 02DS94 | 02DS96 | 02DS97 |
|---|---|---|---|---|---|---|---|---|---|
| Mineral | plag | plag | plag | plag | plag | plag | plag | plag | plag |
| No Analyses | 2 | 2 | 2 | 1 | 2 | 2 | 2 | 2 | 2 |
| Rock Type | 1 | 1 | 2 | 1 | 2 | 3 | 2 or 3 | 1 or 3 | 5 |
| Area | Engagement Zone | Engagement Zone | Engagement Zone | Cristal | Cristal | GQ Diamond Discovery | Heterolithic Breccia | Heterolithic Breccia | Fine grained dike |
| Easting | 667729 | 667729 | 667729 | 666482 | 666482 | 665570 | 656724 | 656022 | 656022 |
| Northing | 5336050 | 5336050 | 5336050 | 5337338 | 5337338 | 5333068 | 5340156 | 5340393 | 5340393 |
| SiO2 | 67.72 | 68.19 | 67.69 | 67.11 | 67.37 | 68.03 | 67.98 | 68.11 | 54.82 |
| TiO2 | 0.01 | 0.01 | 0.02 | 0.05 | 0.02 | 0.04 | 0.00 | 0.02 | 0.05 |
| Al2O3 | 19.10 | 19.66 | 19.82 | 20.82 | 19.88 | 19.35 | 20.02 | 19.35 | 27.08 |
| CaO | 0.22 | 0.43 | 0.57 | 1.20 | 0.76 | 0.29 | 0.87 | 0.22 | 10.69 |
| Fe2O3 | 0.75 | 0.21 | 0.20 | 0.12 | 0.21 | 0.34 | 0.07 | 0.18 | 0.83 |
| Na2O | 10.93 | 11.34 | 11.23 | 10.69 | 11.49 | 11.69 | 11.23 | 11.80 | 5.45 |
| K2O | 0.09 | 0.07 | 0.16 | 0.26 | 0.24 | 0.28 | 0.04 | 0.03 | 0.16 |
| SrO | 0.15 | 0.23 | 0.21 | 0.24 | 0.18 | 0.13 | 0.49 | 0.06 | 0.05 |
| BaO | 0.02 | 0.00 | 0.01 | 0.06 | 0.02 | 0.04 | 0.00 | 0.00 | 0.04 |
| Total | 99.00 | 100.14 | 99.90 | 100.53 | 100.17 | 100.18 | 100.71 | 99.77 | 99.17 |
| **Cations on the basis of 32 O** | | | | | | | | | |
| Si | 11.968 | 11.923 | 11.876 | 11.722 | 11.820 | 11.921 | 11.851 | 11.950 | 10.001 |
| Ti | 0.002 | 0.001 | 0.003 | 0.006 | 0.003 | 0.005 | 0.000 | 0.002 | 0.007 |
| Al | 3.979 | 4.051 | 4.097 | 4.285 | 4.112 | 3.996 | 4.112 | 4.002 | 5.821 |
| Ca | 0.042 | 0.080 | 0.106 | 0.224 | 0.143 | 0.055 | 0.162 | 0.041 | 2.089 |
| Fe3+ | 0.099 | 0.028 | 0.026 | 0.016 | 0.028 | 0.045 | 0.010 | 0.024 | 0.114 |
| Na | 3.746 | 3.845 | 3.820 | 3.620 | 3.910 | 3.972 | 3.797 | 4.013 | 1.929 |
| K | 0.021 | 0.016 | 0.035 | 0.057 | 0.053 | 0.062 | 0.010 | 0.007 | 0.038 |
| Sr | 0.015 | 0.023 | 0.021 | 0.024 | 0.018 | 0.013 | 0.050 | 0.006 | 0.005 |
| Ba | 0.001 | 0.000 | 0.001 | 0.004 | 0.001 | 0.003 | 0.000 | 0.000 | 0.003 |
| Charge | 64 | 64 | 64 | 64 | 64 | 64 | 64 | 64 | 64 |
| Albite % | 97.93 | 97.01 | 95.90 | 92.13 | 94.78 | 96.78 | 94.50 | 98.66 | 47.46 |
| Anorthite % | 1.49 | 2.59 | 3.21 | 6.30 | 3.90 | 1.66 | 5.25 | 1.16 | 51.53 |
| Orthoclase % | 0.58 | 0.40 | 0.89 | 1.57 | 1.32 | 1.56 | 0.24 | 0.18 | 1.01 |

**Rock Type Codes**

1 Breccia matrix

2 Fine breccia

3 lamprophyre dike

5 diabase dike

**Table 4:** Amphibole analyses.

| Sample | 02DS86 | 02DS86 | 02DS87 | 02DS87-402 | 02DS88 | 02DS88 | 02DS89-420 | 02DS89 | 02DS90-427 | 02DS90-429 |
|---|---|---|---|---|---|---|---|---|---|---|
| No. Analyses | av of 3 | av of 4 | av of 2 | 1 | av of 3 | av of 3 | 1 | av of 3 | 1 | 1 |
| Mineral | phenocryst | common amp | amp pheno | actin blade | low Al amph | actinolite | hi Al amp | low Al amp | mod Al amp | hi Al amp |
| Rock Type | 1 | 1 | 1 | 1 | 2 | 2 | 1 | 1 | 2 | 2 |
| Area | Engagement Zone | Engagement Zone | Engagement Zone | Engagement Zone | Engagement Zone | Engagement Zone | Cristal | Cristal | Cristal | Cristal |
| Easting | 667729 | 667729 | 667729 | 667729 | 667729 | 667729 | 666482 | 666482 | 666482 | 666482 |
| Northing | 5336050 | 5336050 | 5336050 | 5336050 | 5336050 | 5336050 | 5337338 | 5337338 | 5337338 | 5337338 |
| SiO2 | 43.02 | 55.22 | 43.20 | 55.90 | 50.02 | 54.47 | 42.23 | 54.11 | 49.75 | 41.73 |
| TiO2 | 1.62 | 0.05 | 1.70 | 0.00 | 0.53 | 0.03 | 2.41 | 0.21 | 0.06 | 0.14 |
| Al2O3 | 10.92 | 0.95 | 11.33 | 0.44 | 4.78 | 1.42 | 13.85 | 1.98 | 5.40 | 11.99 |
| Cr2O3 | 0.09 | 0.08 | 0.01 | 0.34 | 0.23 | 0.09 | 0.00 | 0.04 | 0.06 | 0.07 |
| FeO* | 11.38 | 7.09 | 10.45 | 5.86 | 11.75 | 8.81 | 11.39 | 8.67 | 14.67 | 18.71 |
| MnO | 0.18 | 0.16 | 0.16 | 0.10 | 0.27 | 0.22 | 0.21 | 0.26 | 0.30 | 0.32 |
| MgO | 14.81 | 19.44 | 15.55 | 20.44 | 15.14 | 18.34 | 13.14 | 18.47 | 14.96 | 15.19 |
| NiO | 0.00 | 0.00 | 0.00 | 0.00 | 0.00 | 0.00 | 0.00 | 0.00 | 0.00 | 0.00 |
| CaO | 10.95 | 13.01 | 10.80 | 13.20 | 12.20 | 13.11 | 10.51 | 12.54 | 10.24 | 6.71 |
| Na2O | 2.28 | 0.14 | 2.44 | 0.16 | 0.69 | 0.11 | 1.16 | 0.18 | 0.22 | 0.06 |
| K2O | 0.91 | 0.04 | 0.84 | 0.03 | 0.24 | 0.07 | 1.11 | 0.04 | 0.05 | 0.31 |
| F | 0.13 | 0.05 | 0.27 | 0.06 | 0.08 | 0.05 | 0.06 | 0.07 | 0.04 | 0.04 |
| Cl | 0.00 | 0.01 | 0.00 | 0.01 | 0.03 | 0.00 | 0.00 | 0.00 | 0.05 | 0.00 |
| Total | 96.29 | 96.22 | 96.75 | 96.53 | 95.96 | 96.73 | 96.08 | 96.57 | 95.79 | 95.26 |
| O_F | 0.05 | 0.02 | 0.11 | 0.03 | 0.03 | 0.02 | 0.03 | 0.03 | 0.02 | 0.02 |
| O_Cl | 0.00 | 0.00 | 0.00 | 0.00 | 0.01 | 0.00 | 0.00 | 0.00 | 0.01 | 0.00 |
| O_F_Cl | 0.05 | 0.02 | 0.11 | 0.03 | 0.04 | 0.02 | 0.03 | 0.03 | 0.03 | 0.02 |
| Fe2O3 calc | 4.43 | 0.86 | 4.70 | 0.65 | 1.79 | 1.49 | 4.26 | 1.73 | 3.93 | 13.78 |
| FeO calc | 7.39 | 6.32 | 6.22 | 5.28 | 10.14 | 7.47 | 7.56 | 7.11 | 11.13 | 6.31 |
| H2O calc | 1.97 | 2.08 | 1.92 | 2.09 | 2.00 | 2.07 | 2.01 | 2.07 | 2.01 | 2.01 |
| Total | 98.65 | 98.36 | 99.02 | 98.66 | 98.10 | 98.93 | 98.49 | 98.77 | 98.16 | 98.64 |
| | | | | | | | | | | |
| Formula average of min and max Fe3+ (Leake et al. 1997) | | | | | | | | | | |
| Si | 6.350 | 7.853 | 6.317 | 7.888 | 7.339 | 7.769 | 6.204 | 7.712 | 7.302 | 6.147 |
| Al(iv) | 1.650 | 0.147 | 1.683 | 0.074 | 0.661 | 0.231 | 1.796 | 0.288 | 0.698 | 1.853 |
| Sum T | 8.000 | 8.000 | 8.000 | 7.961 | 8.000 | 8.000 | 8.000 | 8.000 | 8.000 | 8.000 |
| | | | | | | | | | | |
| Al(vi) | 0.250 | 0.011 | 0.270 | 0.000 | 0.166 | 0.007 | 0.602 | 0.046 | 0.235 | 0.228 |
| Ti | 0.180 | 0.005 | 0.187 | 0.000 | 0.059 | 0.003 | 0.266 | 0.023 | 0.006 | 0.016 |
| Fe3+ | 0.492 | 0.092 | 0.517 | 0.069 | 0.198 | 0.160 | 0.472 | 0.186 | 0.434 | 1.528 |
| Cr | 0.011 | 0.007 | 0.001 | 0.038 | 0.027 | 0.010 | 0.000 | 0.004 | 0.007 | 0.008 |
| Mg | 3.259 | 4.122 | 3.389 | 4.299 | 3.311 | 3.900 | 2.879 | 3.924 | 3.272 | 3.220 |
| Ni | 0.000 | 0.000 | 0.000 | 0.000 | 0.000 | 0.000 | 0.000 | 0.000 | 0.000 | 0.000 |
| Fe2+ | 0.809 | 0.752 | 0.636 | 0.594 | 1.240 | 0.891 | 0.782 | 0.818 | 1.045 | 0.000 |
| Mn | 0.000 | 0.011 | 0.000 | 0.000 | 0.000 | 0.027 | 0.000 | 0.000 | 0.000 | 0.000 |
| Sum C (M1,M2,M3) | 5.000 | 5.000 | 5.000 | 5.000 | 5.000 | 4.998 | 5.000 | 5.000 | 5.000 | 5.000 |
| | | | | | | | | | | |
| Mg | 0.000 | 0.000 | 0.000 | 0.000 | 0.000 | 0.000 | 0.000 | 0.000 | 0.000 | 0.116 |
| Ni | 0.000 | 0.000 | 0.000 | 0.000 | 0.000 | 0.000 | 0.000 | 0.000 | 0.000 | 0.000 |
| Fe2+ | 0.104 | 0.000 | 0.125 | 0.029 | 0.005 | 0.000 | 0.146 | 0.029 | 0.322 | 0.777 |
| Mn | 0.022 | 0.008 | 0.020 | 0.011 | 0.034 | 0.000 | 0.026 | 0.031 | 0.037 | 0.040 |
| Ca | 1.732 | 1.983 | 1.692 | 1.996 | 1.918 | 2.004 | 1.655 | 1.915 | 1.610 | 1.059 |
| Na | 0.143 | 0.009 | 0.163 | 0.000 | 0.044 | 0.000 | 0.174 | 0.025 | 0.032 | 0.008 |
| Sum B (M4) | 2.000 | 2.000 | 2.000 | 2.037 | 2.000 | 2.004 | 2.000 | 2.000 | 2.000 | 2.000 |
| | | | | | | | | | | |
| Na | 0.509 | 0.029 | 0.529 | 0.043 | 0.151 | 0.031 | 0.157 | 0.025 | 0.032 | 0.008 |
| K | 0.171 | 0.007 | 0.156 | 0.005 | 0.046 | 0.012 | 0.208 | 0.007 | 0.009 | 0.058 |
| Sum A | 0.680 | 0.036 | 0.685 | 0.048 | 0.197 | 0.043 | 0.365 | 0.032 | 0.041 | 0.066 |
| | | | | | | | | | | |
| F | 0.059 | 0.021 | 0.127 | 0.029 | 0.036 | 0.024 | 0.029 | 0.033 | 0.021 | 0.020 |
| Cl | 0.001 | 0.002 | 0.000 | 0.001 | 0.007 | 0.001 | 0.000 | 0.000 | 0.012 | 0.001 |
| OH | 1.939 | 1.977 | 1.873 | 1.970 | 1.957 | 1.975 | 1.971 | 1.966 | 1.968 | 1.979 |
| Sum OH | 2.000 | 2.000 | 2.000 | 2.000 | 2.000 | 2.000 | 2.000 | 2.000 | 2.000 | 2.000 |
| Sum_cat | 15.680 | 15.036 | 15.685 | 15.046 | 15.197 | 15.045 | 15.365 | 15.032 | 15.041 | 15.066 |
| Mineral Name | magnesio-hastingsite | actinolite | magnesio-hastingsite | actinolite | magnesio-hornblende | actinolite | tschermakite | actinolite | magnesio-hornblende | calcic amphibole |

Table 4: continued.

| Sample | 02DS91-436 | 02DS91-437 | 02DS94 | 02DS94-462 | 02DS94-458 | 02DS94-459 | 02DS95 |
|---|---|---|---|---|---|---|---|
| No. Analyses | 1 | 1 | av of 2 | 1 | 1 | 1 | av of 2 |
| Mineral | lo Al amp | lo Al amp | Al amph | mod Al | mod Al | lo Al | Al amp |
| Rock Type | 3 | 3 | 2 or 3 | 2 or 3 | 2 or 3 | 2 or 3 | 2 or 3 |
| Area | GQ Diamond Discovery | GQ Diamond Discovery | Heterolithic Breccia | Heterolithic Breccia | Heterolithic Breccia | Heterolithic Breccia | Giant Inclusion Breccia |
| Easting | 665570 | 665570 | 656724 | 656724 | 656724 | 656724 | 656440 |
| Northing | 5333068 | 5333068 | 5340156 | 5340156 | 5340156 | 5340156 | 5340375 |
| SiO2 | 55.74 | 54.48 | 45.37 | 51.97 | 53.39 | 55.53 | 48.43 |
| TiO2 | 0.04 | 0.10 | 0.86 | 0.27 | 0.02 | 0.06 | 0.56 |
| Al2O3 | 0.91 | 2.06 | 10.83 | 5.44 | 4.18 | 1.17 | 7.98 |
| Cr2O3 | 0.10 | 0.01 | 0.06 | 0.13 | 0.00 | 0.03 | 0.21 |
| FeO* | 7.46 | 8.41 | 13.68 | 10.35 | 9.39 | 7.45 | 13.09 |
| MnO | 0.18 | 0.20 | 0.22 | 0.22 | 0.25 | 0.20 | 0.22 |
| MgO | 18.96 | 18.11 | 13.26 | 16.58 | 17.66 | 19.79 | 13.87 |
| NiO | 0.00 | 0.00 | 0.00 | 0.00 | 0.00 | 0.00 | 0.00 |
| CaO | 12.88 | 12.55 | 11.53 | 12.27 | 12.26 | 12.59 | 11.87 |
| Na2O | 0.15 | 0.32 | 1.32 | 0.76 | 0.67 | 0.22 | 0.97 |
| K2O | 0.04 | 0.13 | 0.64 | 0.15 | 0.07 | 0.03 | 0.44 |
| F | 0.00 | 0.09 | 0.08 | 0.09 | 0.00 | 0.00 | 0.05 |
| Cl | 0.00 | 0.00 | 0.00 | 0.00 | 0.00 | 0.00 | 0.01 |
| Total | 96.45 | 96.47 | 97.86 | 98.23 | 97.89 | 97.07 | 97.69 |
| O_F | 0.00 | 0.04 | 0.03 | 0.04 | 0.00 | 0.00 | 0.02 |
| O_Cl | 0.00 | 0.00 | 0.00 | 0.00 | 0.00 | 0.00 | 0.00 |
| O_F_Cl | 0.00 | 0.04 | 0.03 | 0.04 | 0.00 | 0.00 | 0.02 |
| Fe2O3 calc | 0.16 | 0.70 | 4.68 | 2.05 | 2.15 | 1.46 | 2.50 |
| FeO calc | 7.31 | 7.78 | 9.47 | 8.50 | 7.45 | 6.13 | 10.84 |
| H2O calc | 2.11 | 2.05 | 2.03 | 2.07 | 2.13 | 2.13 | 2.04 |
| Total | 98.58 | 98.56 | 100.32 | 100.47 | 100.23 | 99.35 | 99.96 |
| **Formula average of min and max Fe3+ (Leake et al. 1997)** | | | | | | | |
| Si | 7.916 | 7.780 | 6.586 | 7.359 | 7.523 | 7.815 | 7.017 |
| Al(iv) | 0.084 | 0.220 | 1.414 | 0.641 | 0.477 | 0.185 | 0.983 |
| Sum T | 8.000 | 8.000 | 8.000 | 8.000 | 8.000 | 8.000 | 8.000 |
| Al(vi) | 0.068 | 0.127 | 0.439 | 0.267 | 0.216 | 0.009 | 0.380 |
| Ti | 0.004 | 0.011 | 0.093 | 0.029 | 0.002 | 0.007 | 0.061 |
| Fe3+ | 0.017 | 0.075 | 0.511 | 0.219 | 0.228 | 0.155 | 0.272 |
| Cr | 0.011 | 0.001 | 0.007 | 0.015 | 0.000 | 0.003 | 0.024 |
| Mg | 4.014 | 3.855 | 2.869 | 3.500 | 3.710 | 4.152 | 2.996 |
| Ni | 0.000 | 0.000 | 0.000 | 0.000 | 0.000 | 0.000 | 0.000 |
| Fe2+ | 0.869 | 0.929 | 1.080 | 0.970 | 0.842 | 0.674 | 1.267 |
| Mn | 0.017 | 0.003 | 0.000 | 0.000 | 0.000 | 0.000 | 0.000 |
| Sum C (M1,M2,M3) | 5.000 | 5.000 | 5.000 | 5.000 | 5.000 | 5.000 | 5.000 |
| Mg | 0.000 | 0.000 | 0.000 | 0.000 | 0.000 | 0.000 | 0.000 |
| Ni | 0.000 | 0.000 | 0.000 | 0.000 | 0.000 | 0.000 | 0.000 |
| Fe2+ | 0.000 | 0.000 | 0.070 | 0.036 | 0.035 | 0.047 | 0.047 |
| Mn | 0.005 | 0.021 | 0.027 | 0.026 | 0.030 | 0.024 | 0.027 |
| Ca | 1.960 | 1.921 | 1.793 | 1.861 | 1.851 | 1.899 | 1.843 |
| Na | 0.035 | 0.058 | 0.110 | 0.076 | 0.084 | 0.029 | 0.084 |
| Sum B (M4) | 2.000 | 2.000 | 2.000 | 2.000 | 2.000 | 2.000 | 2.000 |
| Na | 0.007 | 0.031 | 0.262 | 0.131 | 0.099 | 0.030 | 0.168 |
| K | 0.007 | 0.024 | 0.119 | 0.028 | 0.013 | 0.005 | 0.080 |
| Sum A | 0.014 | 0.055 | 0.380 | 0.159 | 0.112 | 0.034 | 0.268 |
| F | 0.000 | 0.043 | 0.036 | 0.040 | 0.000 | 0.000 | 0.024 |
| Cl | 0.000 | 0.000 | 0.001 | 0.001 | 0.000 | 0.000 | 0.003 |
| OH | 2.000 | 1.957 | 1.963 | 1.960 | 2.000 | 2.000 | 1.973 |
| Sum OH | 2.000 | 2.000 | 2.000 | 2.000 | 2.000 | 2.000 | 2.000 |
| Sum_cat | 15.014 | 15.055 | 15.380 | 15.159 | 15.112 | 15.034 | 15.268 |
| Mineral Name | actinolite | actinolite | magnesio-hornblende | magnesio-hornblende | actinolite | actinolite | magnesio-hornblende |

**Rock Type Codes**

1 Breccia matrix
2 Fine breccia
3 Lamprophyre dike

T, C, M1, M2, M3, B, M4 and A refer to atomic sites in the amphibole molecule.

**Table 5:** Mica analyses.

| Sample | 02DS88-410 | 02DS90-428 | 02DS90-430 | 02DS91 | 02DS94 | 02DS95 | 02DS96 | |
|---|---|---|---|---|---|---|---|---|
| Mineral | mica | mica | mica | mica | mica | mica | mica | |
| No analyses | 1 | 1 | 1 | av of 2 | av of 2 | av of 2 | av of 2 | |
| Rock Type | 2 | 2 | 2 | 3 | 2 or 3 | 2 or 3 | 1 or 3 | **Rock Type codes** |
| Area | Engagement Zone | Cristal | Cristal | GQ Diamond Discovery | Heterolithic Breccia | Giant Inclusion Breccia | Heterolithic Breccia | 1 Breccia matrix |
| Easting | 667729 | 666482 | 666482 | 665570 | 656724 | 656440 | 656022 | 2 Breccia |
| Northing | 5336050 | 5337338 | 5337338 | 5333068 | 5340156 | 5340375 | 5340393 | 3 Lamprophyre dike |
| SiO2 | 43.46 | 37.34 | 37.35 | 38.57 | 38.51 | 37.51 | 37.38 | |
| TiO2 | 0.41 | 1.13 | 0.68 | 1.46 | 1.68 | 1.75 | 1.90 | |
| Al2O3 | 26.28 | 17.63 | 16.05 | 14.98 | 16.28 | 16.83 | 16.14 | |
| Cr2O3 | 0.15 | 0.02 | 0.04 | 0.70 | 0.32 | 0.11 | 0.14 | |
| MgO | 4.72 | 11.28 | 12.71 | 15.26 | 16.09 | 14.99 | 14.08 | |
| CaO | 0.02 | 0.18 | 2.41 | 0.09 | 0.02 | 0.02 | 0.01 | |
| MnO | 0.06 | 0.19 | 0.25 | 0.10 | 0.10 | 0.13 | 0.04 | |
| FeO | 6.05 | 19.02 | 19.44 | 13.80 | 13.26 | 14.48 | 15.62 | |
| Na2O | 0.04 | 0.02 | 0.01 | 0.03 | 0.08 | 0.07 | 0.10 | |
| K2O | 10.04 | 9.40 | 4.85 | 8.55 | 8.44 | 8.90 | 8.92 | |
| F | 0.08 | 0.03 | 0.07 | 0.09 | 0.14 | 0.18 | 0.10 | |
| Cl | 0.00 | 0.00 | 0.00 | 0.01 | 0.02 | 0.02 | 0.00 | |
| H2O | 4.13 | 3.98 | 3.93 | 3.95 | 4 | 3.94 | 3.94 | |
| Total | 95.42 | 100.21 | 97.80 | 97.58 | 98.93 | 98.93 | 98.36 | |
| F=O | 0.03 | 0.01 | 0.03 | 0.04 | 0.06 | 0.08 | 0.04 | |
| Cl=O | 0.00 | 0.00 | 0.00 | 0.00 | 0.00 | 0.00 | 0.00 | |
| Total | 95.37 | 100.19 | 97.76 | 97.52 | 98.83 | 98.81 | 98.30 | |
| **Cations on the basis of 24(O,OH,F,Cl) with OH+F+Cl=4; all Fe assumed to be FeO** | | | | | | | | |
| Si | 6.257 | 5.601 | 5.657 | 5.788 | 5.672 | 5.58 | 5.625 | tetra and octo refer to the tetrahedral and octohedral sites in the mica molecule |
| Al(iv) | 1.743 | 2.399 | 2.343 | 2.212 | 2.328 | 2.42 | 2.375 | |
| Sum tetra | 8 | 8 | 8 | 8 | 8 | 8 | 8 | |
| Al(vi) | 2.713 | 0.715 | 0.52 | 0.435 | 0.496 | 0.529 | 0.485 | |
| Ti | 0.044 | 0.127 | 0.077 | 0.165 | 0.186 | 0.196 | 0.215 | |
| Fe3 | 0 | 0 | 0 | 0 | 0 | 0 | 0 | |
| Fe2 | 0.728 | 2.386 | 2.462 | 1.732 | 1.633 | 1.802 | 1.966 | |
| Cr | 0.017 | 0.002 | 0.005 | 0.083 | 0.037 | 0.013 | 0.017 | |
| Mn | 0.007 | 0.024 | 0.032 | 0.013 | 0.012 | 0.016 | 0.005 | |
| Mg | 1.013 | 2.522 | 2.87 | 3.414 | 3.533 | 3.325 | 3.158 | |
| Sum octo | 4.522 | 5.776 | 5.966 | 5.842 | 5.897 | 5.881 | 5.846 | |
| Ca | 0.003 | 0.029 | 0.391 | 0.014 | 0.003 | 0.003 | 0.002 | |
| Na | 0.011 | 0.006 | 0.003 | 0.009 | 0.023 | 0.02 | 0.029 | |
| K | 1.844 | 1.799 | 0.937 | 1.637 | 1.586 | 1.689 | 1.712 | |
| sum | 1.858 | 1.834 | 1.331 | 1.66 | 1.612 | 1.712 | 1.743 | |
| Cations | 14.38 | 15.61 | 15.297 | 15.502 | 15.509 | 15.593 | 15.589 | |
| CF | 0.073 | 0.028 | 0.067 | 0.085 | 0.13 | 0.169 | 0.095 | |
| CCl | 0 | 0 | 0 | 0.005 | 0.01 | 0.01 | 0 | |
| OH | 3.964 | 3.986 | 3.966 | 3.955 | 3.93 | 3.91 | 3.952 | |
| O | 24 | 24 | 24 | 24 | 24 | 24 | 24 | |
| Fe/(Fe+Mg) | 0.42 | 0.49 | 0.46 | 0.34 | 0.32 | 0.35 | 0.38 | |
| Mg/(Fe+Mg) | 0.58 | 0.51 | 0.54 | 0.66 | 0.68 | 0.65 | 0.62 | |
| Name | biotite | biotite | biotite | biotite | phlogopite | biotite | biotite | |

Table 6: Pyroxene analyses.

| Sample | 02DS89-426 | 02DS97-485 | 02DS97-486 |
|---|---|---|---|
| Mineral | cpx | augite | augite |
| No analyses | 1 | 1 | 1 |
| Rock Type | 1 | 5 | 5 |
| Area | Cristal | Diabase dike | Diabase dike |
| Easting | 666482 | 656022 | 656022 |
| Northing | 5337338 | 5340393 | 5340393 |
| | | | |
| SiO2 | 51.90 | 50.08 | 49.61 |
| TiO2 | 0.34 | 0.86 | 0.69 |
| Al2O3 | 1.56 | 3.19 | 3.51 |
| Cr2O3 | 0.15 | 0.00 | 0.11 |
| MgO | 16.43 | 13.82 | 14.26 |
| CaO | 22.35 | 11.92 | 18.24 |
| MnO | 0.16 | 0.46 | 0.26 |
| FeO | 5.58 | 18.92 | 11.75 |
| Na2O | 0.43 | 0.22 | 0.26 |
| K2O | 0.00 | 0.41 | 0.00 |
| Total | 98.89 | 99.87 | 98.69 |
| Cations on the basis of 6 Oxygen | | | |
| TSi | 1.919 | 1.908 | 1.877 |
| TAl | 0.068 | 0.092 | 0.123 |
| TFe3 | 0.013 | 0 | 0 |
| Sum T | 2 | 2 | 2 |
| | | | |
| M1Al | 0 | 0.051 | 0.034 |
| M1Ti | 0.009 | 0.025 | 0.02 |
| M1Fe3 | 0.088 | 0.027 | 0.065 |
| M1Fe2 | 0 | 0.112 | 0.074 |
| M1Cr | 0.004 | 0 | 0.003 |
| M1Mg | 0.898 | 0.785 | 0.804 |
| Sum (M1) | 0.999 | 1 | 1 |
| | | | |
| M2Mg | 0.007 | 0 | 0 |
| M2Fe2 | 0.072 | 0.463 | 0.233 |
| M2Mn | 0.005 | 0.015 | 0.008 |
| M2Ca | 0.886 | 0.486 | 0.74 |
| M2Na | 0.03 | 0.016 | 0.019 |
| M2K | 0 | 0.02 | 0 |
| Sum (M2) | 1 | 1 | 1 |
| | | | |
| Sum_cat | 4 | 3.98 | 4 |
| | | | |
| X Ca | 47.409 | 26.129 | 39.776 |
| X Mg | 48.488 | 42.161 | 43.26 |
| X $Fe^{2+}$+Mn | 4.102 | 31.71 | 16.963 |
| | | | |
| Name | diopside | augite | augite |

**Rock Type Codes**

1 Breccia matrix
5 Diabase dike

T, M1 and M2 refer to atomic sites in the pyroxene molecule

X = mole fraction

**Table 7:** Chlorite analyses.

| Sample | 02DS86-390 | 02DS86-395 | 02DS86-387 | 02DS87-403 | 02DS87-404 | 02DS88-407 | 02DS89-418 | 02DS91-433 | 02DS91-434 | 02DS93-449 | 02DS95-465 | 02DS95-468 |
|---|---|---|---|---|---|---|---|---|---|---|---|---|
| Mineral | chlorite | chlorite | chlorite | chlorite | chlorite | chlorite | chlorite | chlorite | chlorite | chlorite | chlorite | chlorite |
| No. Analyses | 1 | 1 | 1 | 1 | 1 | 1 | 1 | 1 | 1 | 1 | 1 | 1 |
| Rock Type | 1 | 1 | 1 | 1 | 1 | 2 | 1 | 3 | 3 | 3 | 2 or 3 | 2 or 3 |
| Area | Engagement Zone | Engagement Zone | Engagement Zone | Engagement Zone | Engagement Zone | Engagement Zone | Cristal | GQ Diamond Discovery | GQ Diamond Discovery | Lamprophyre Dike (A Star) | Giant Inclusion Breccia | Giant Inclusion Breccia |
| Easting | 667729 | 667729 | 667729 | 667729 | 667729 | 667729 | 666482 | 665570 | 665570 | 657140 | 656440 | 656440 |
| Northing | 5336050 | 5336050 | 5336050 | 5336050 | 5336050 | 5336050 | 5337338 | 5333068 | 5333068 | 5340023 | 5340375 | 5340375 |
| SiO2 | 28.457 | 27.[illegible]6 | 27.813 | 28.306 | 27.929 | 27.299 | 29.349 | 29.029 | 26.793 | 27.725 | 27.395 | 27.767 |
| TiO2 | 0.019 | 0.[illegible]15 | 0.013 | 0.032 | 0.035 | 0.013 | 0.000 | 0.139 | 0.058 | 0.000 | 0.108 | 0.086 |
| Al2O3 | 20.493 | 20.798 | 20.274 | 20.525 | 20.338 | 21.828 | 19.972 | 20.218 | 21.294 | 20.413 | 22.154 | 22.278 |
| Cr2O3 | 0.385 | 0.413 | 0.901 | 0.975 | 0.340 | 0.179 | 0.187 | 0.229 | 0.208 | 0.583 | 0.097 | 0.096 |
| MgO | 22.564 | 22.628 | 22.724 | 23.477 | 22.151 | 19.317 | 24.083 | 21.769 | 21.711 | 24.657 | 21.963 | 21.948 |
| CaO | 0.068 | 0.023 | 0.065 | 0.007 | 0.246 | 0.124 | 0.023 | 0.011 | 0.037 | 0.023 | 0.036 | 0.005 |
| MnO | 0.209 | 0.219 | 0.194 | 0.205 | 0.205 | 0.289 | 0.194 | 0.172 | 0.207 | 0.137 | 0.200 | 0.213 |
| FeO | 15.266 | 15.185 | 15.294 | 14.649 | 14.695 | 18.899 | 13.406 | 15.791 | 16.105 | 12.472 | 16.510 | 16.819 |
| Na2O | 0.004 | 0.000 | 0.000 | 0.000 | 0.000 | 0.000 | 0.000 | 0.000 | 0.000 | 0.000 | 0.000 | 0.000 |
| K2O | 0.004 | 0.014 | 0.086 | 0.013 | 0.022 | 0.019 | 0.000 | 0.485 | 0.007 | 0.065 | 0.019 | 0.000 |
| F | 0.039 | 0.039 | 0.026 | 0.000 | 0.066 | 0.025 | 0.066 | 0.156 | 0.077 | 0.027 | 0.088 | 0.015 |
| Cl | 0.027 | 0.000 | 0.000 | 0.000 | 0.014 | 0.007 | 0.018 | 0.000 | 0.000 | 0.007 | 0.000 | 0.011 |
| Total | 87.535 | 87.100 | 87.390 | 88.189 | 86.041 | 87.999 | 87.298 | 87.999 | 86.497 | 86.109 | 88.570 | 89.238 |
| H2O calc | 11.94 | 11.99 | 11.93 | 12.13 | 11.79 | 11.84 | 12.09 | 11.96 | 11.75 | 11.95 | 12.04 | 12.17 |
| O=F+Cl | 0.023 | 0.016 | 0.011 | 0.000 | 0.031 | 0.012 | 0.032 | 0.066 | 0.032 | 0.013 | 0.037 | 0.009 |
| Total | 99.432 | 99.067 | 99.305 | 100.319 | 97.782 | 99.819 | 99.336 | 99.869 | 98.202 | 98.038 | 100.559 | 101.391 |
| **Cations on the basis of 36 (O,OH,F,Cl) with OH+F+CL=16; all Fe as FeO** | | | | | | | | | | | | |
| Si | 5.582 | 5.679 | 5.574 | 5.599 | 5.665 | 5.522 | 5.806 | 5.789 | 5.451 | 5.561 | 5.44 | 5.47 |
| Al(iv) | 2.418 | 2.321 | 2.426 | 2.401 | 2.335 | 2.478 | 2.194 | 2.211 | 2.549 | 2.439 | 2.56 | 2.53 |
| Sum_T | 8 | 8 | 8 | 8 | 8 | 8 | 8 | 8 | 8 | 8 | 8 | 8 |
| Al(vi) | 2.374 | 2.496 | 2.491 | 2.38 | 2.523 | 2.722 | 2.459 | 2.537 | 2.553 | 2.382 | 2.621 | 2.638 |
| Ti | 0.002 | 0.003 | 0.002 | 0.005 | 0.005 | 0.002 | 0 | 0.021 | 0.009 | 0 | 0.016 | 0.013 |
| Fe3 | 0 | 0 | 0 | 0 | 0 | 0 | 0 | 0 | 0 | 0 | 0 | 0 |
| Fe2 | 2.567 | 2.548 | 2.549 | 2.423 | 2.493 | 3.197 | 2.218 | 2.633 | 2.74 | 2.092 | 2.742 | 2.771 |
| Cr | 0.143 | 0.061 | 0.065 | 0.152 | 0.054 | 0.029 | 0.029 | 0.036 | 0.033 | 0.092 | 0.015 | 0.015 |
| Mn | 0.033 | 0.035 | 0.037 | 0.034 | 0.035 | 0.05 | 0.033 | 0.029 | 0.036 | 0.023 | 0.034 | 0.036 |
| Mg | 6.799 | 6.713 | 6.772 | 6.923 | 6.698 | 5.825 | 7.102 | 6.471 | 6.585 | 7.372 | 6.501 | 6.445 |
| Ca | 0.014 | 0.015 | 0.005 | 0.001 | 0.053 | 0.027 | 0.005 | 0.002 | 0.008 | 0.005 | 0.008 | 0.001 |
| Na | 0 | 0.002 | 0 | 0 | 0 | 0 | 0 | 0 | 0 | 0 | 0 | 0 |
| K | 0.022 | 0.001 | 0.004 | 0.003 | 0.006 | 0.005 | 0 | 0.123 | 0.002 | 0.017 | 0.005 | 0 |
| Cations | 19.954 | 19.874 | 19.925 | 19.921 | 19.867 | 19.857 | 19.846 | 19.852 | 19.966 | 19.983 | 19.942 | 19.919 |
| CF | 0.033 | 0.049 | 0.05 | 0 | 0.085 | 0.032 | 0.083 | 0.197 | 0.099 | 0.034 | 0.111 | 0.019 |
| CCl | 0 | 0.018 | 0 | 0 | 0.01 | 0.005 | 0.012 | 0 | 0 | 0.005 | 0 | 0.007 |
| OH | 15.983 | 15.966 | 15.975 | 16 | 15.953 | 15.982 | 15.953 | 15.902 | 15.95 | 15.98 | 15.945 | 15.987 |
| O | 36 | 36 | 36 | 36 | 36 | 36 | 36 | 36 | 36 | 36 | 36 | 36 |
| Fe/(Fe+Mg) | 0.27 | 0.28 | 0.27 | 0.26 | 0.27 | 0.35 | 0.24 | 0.29 | 0.29 | 0.22 | 0.3 | 0.3 |
| Mg/(Fe+Mg) | 0.73 | 0.72 | 0.73 | 0.74 | 0.73 | 0.65 | 0.76 | 0.71 | 0.71 | 0.78 | 0.7 | 0.7 |
| Name | Ripidolite | Pycnochlorite | Ripidolite | Ripidolite | Pycnochlorite | Ripidolite | Pycnochlorite | Pycnochlorite | Ripidolite | Ripidolite | Ripidolite | Ripidolite |

**Rock Type Codes**
1 Breccia matrix
2 Breccia
3 Lamprophyre dike

## FELDSPAR

Feldspar compositions within all rock types including lamprophyre dikes, breccia matrix and breccia are albite (Table 3). The only exception is labradorite within the diabase dike (sample 02DS97). Potassium feldspar was not observed in the thin sections.

## AMPHIBOLE

Amphibole is the dominant mafic mineral within most samples and shows considerable compositional variation (Table 4). The dark, pleochroic amphibole macrocrysts within samples of breccia matrix are aluminum-rich calcic amphiboles comprising magnesiohornblende, tschermakite and magnesiohastingsite (Figures 5a, b). The dominant amphibole within the matrix of most rocks is magnesium-rich actinolite. As a group, the amphibole grains show a compositional trend defined by increased Si and decreased Al at fairly constant $Mg/(Mg+Fe^{2+})$ through fields of magnesiohornblende and actinolite (*see* Figure 5b). Textural evidence including actinolite rims on magnesiohornblende grains suggests that this trend represents progressive stages of alteration or metamorphism of magnesiohornblende to actinolite.

## MICA

Mica tends to be concentrated in lamprophyre dikes and breccia fragments more than in the breccia matrix. The available mica analyses (Table 5) from lamprophyre dikes and breccias are magnesium-rich biotite and phlogopite (Figure 6). The mica analyses from breccia at the Cristal occurrence (sample 02DS90) have the highest Fe/(Fe+Mg) ratios, however, these analyses were obtained from mica grains within a felsic clast and do not necessarily reflect the average composition of mica in breccia.

## PYROXENE

The pyroxene inclusion, within an amphibole macrocryst of the breccia matrix, contains elevated CaO and MgO (Table 6) and is classified as diopside (Figure 7). The diopside grain has low Cr and low Na and is characteristic of clinopyroxene crystallized at crustal rather than mantle depths (see discussion of Stone 2001). Pyroxene grains within the diabase dike are augite (Figure 7).

## CHLORITE

Chlorite grains from all samples have high MgO (19.0 to 25.0 weight %) with correspondingly low total iron (12.0 to 19.0 weight %) and high $Al_2O_3$ (20.0 to 22.0 weight %) [Table 7]. Accordingly, chlorite compositions are fairly tightly clustered within fields of ripidolite and pycnochlorite (Figure 8). The magnesium- and aluminum-rich character of chlorite has probably been inherited from magnesiohornblende and related amphiboles through which the chlorite is derived by alteration or metamorphism.

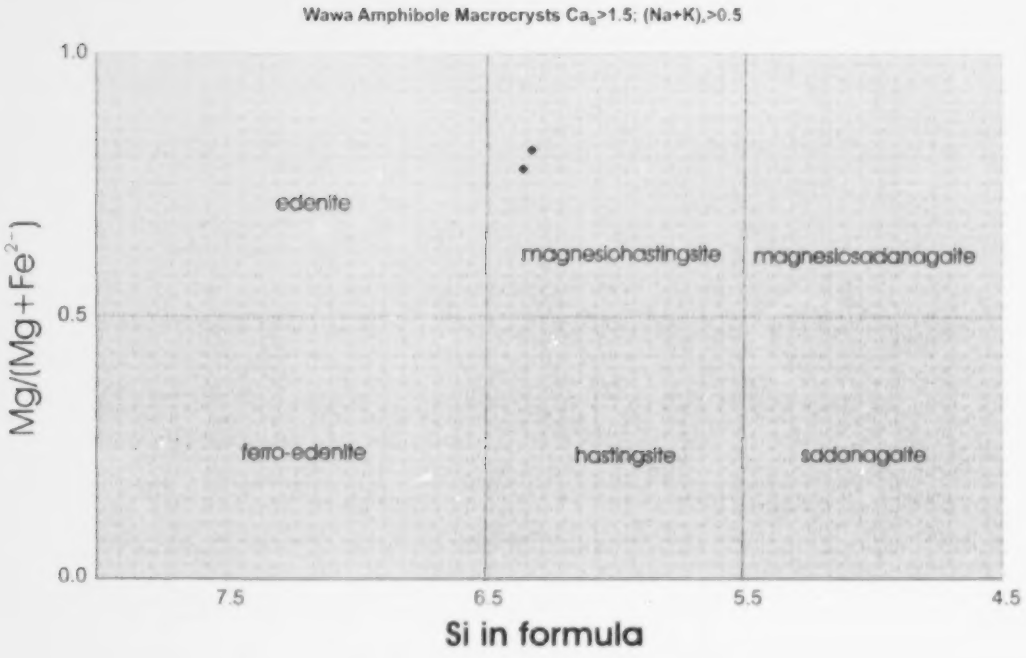


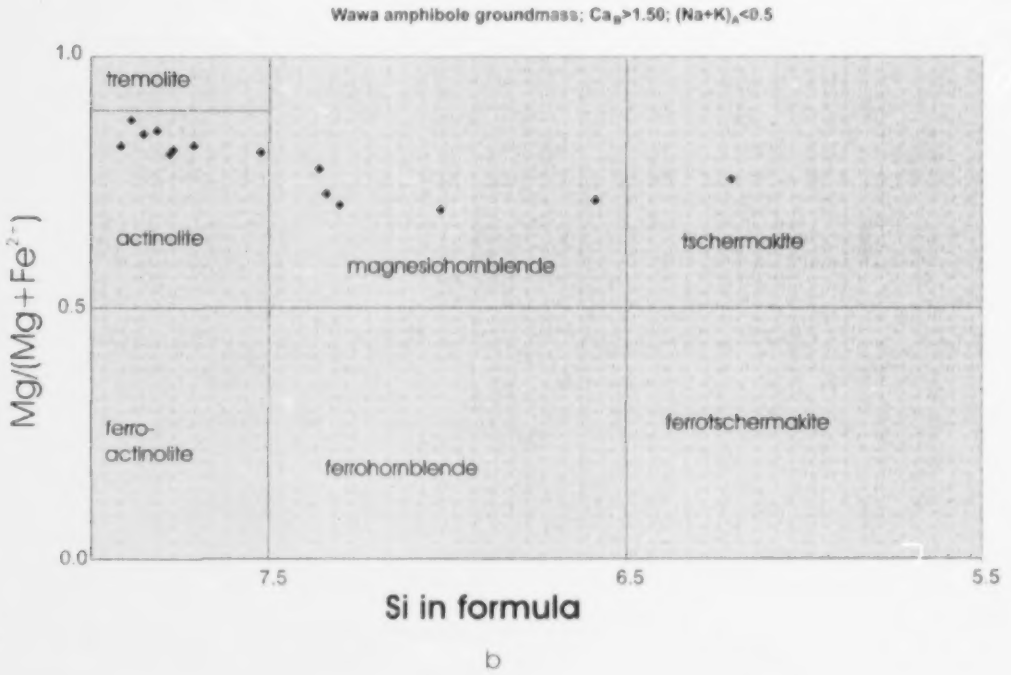


**Figure 5**: Composition of amphiboles (Leake et al. 1997).

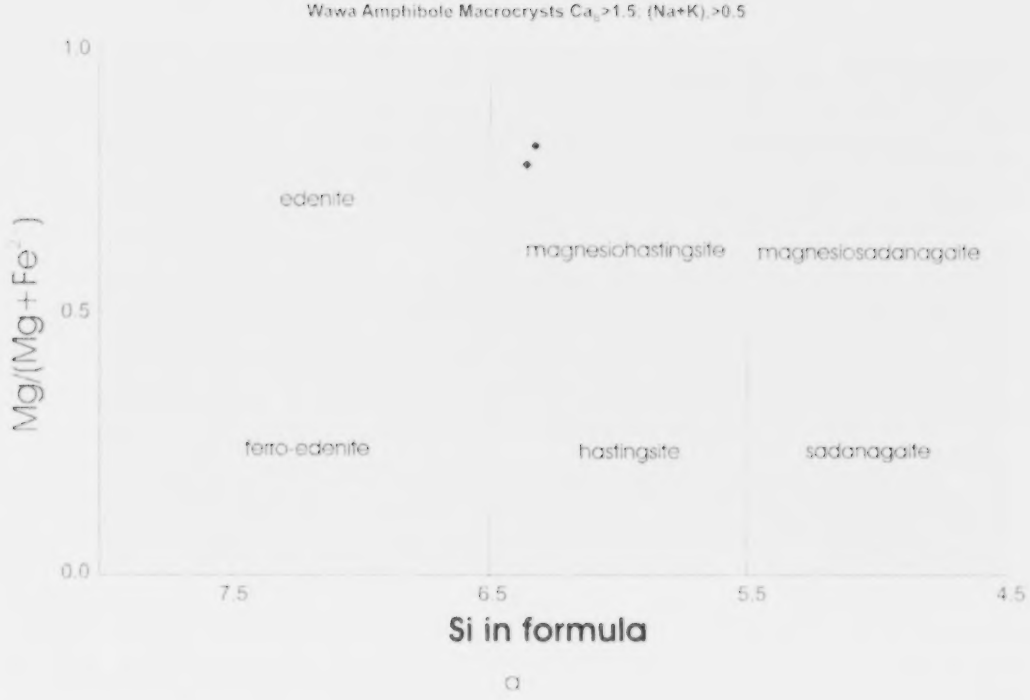


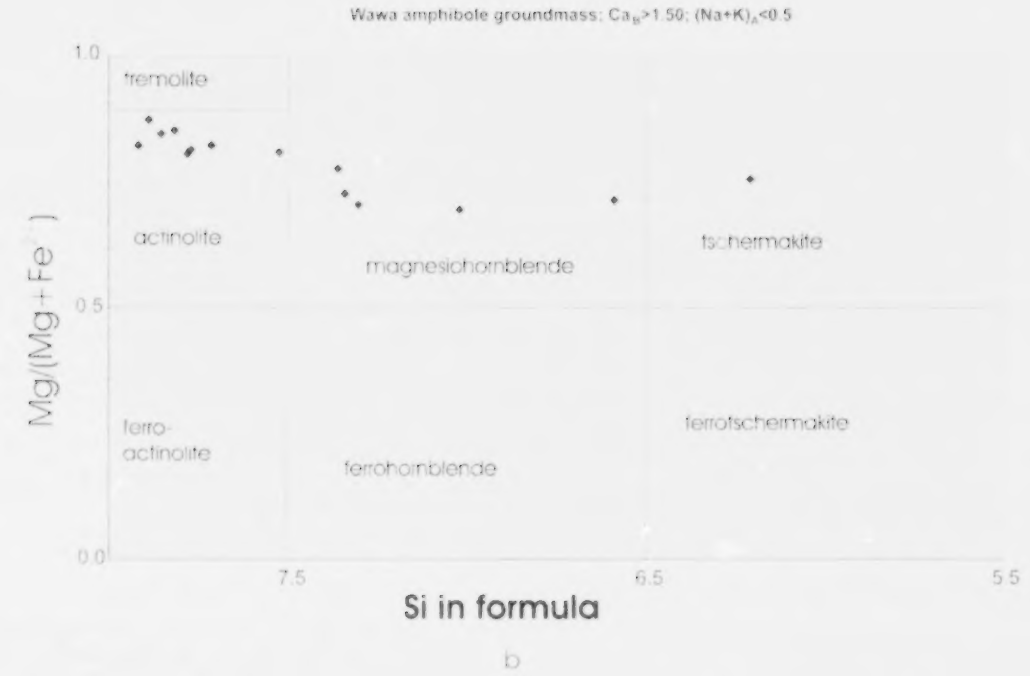


**Figure 5**: Composition of amphiboles (Leake et al. 1997).

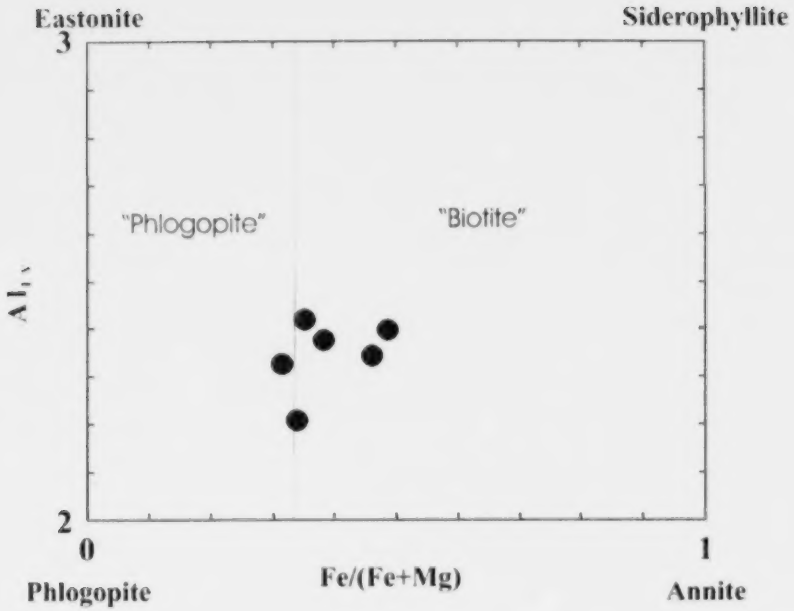


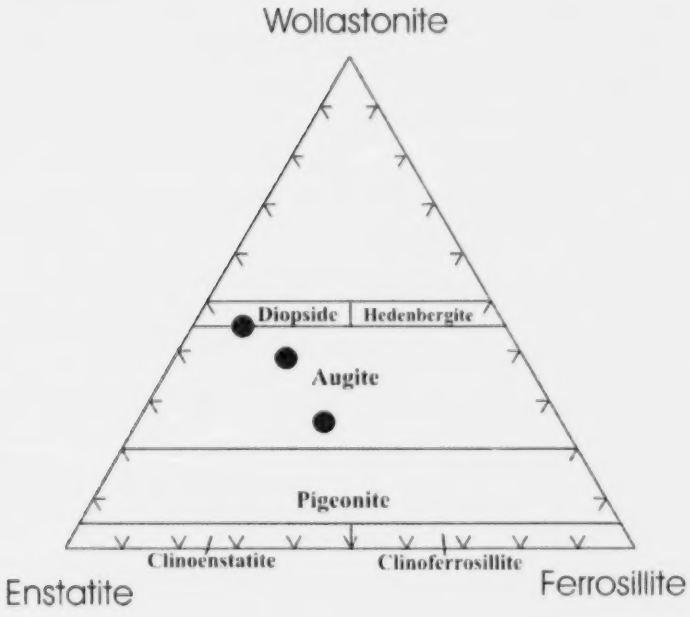


**Figure 6**: (upper) composition of micas. Nomenclature of micas is after Deer, Howie and Zussman (1972).
**Figure 7**: (lower) composition of pyroxenes (Morimoto 1989).

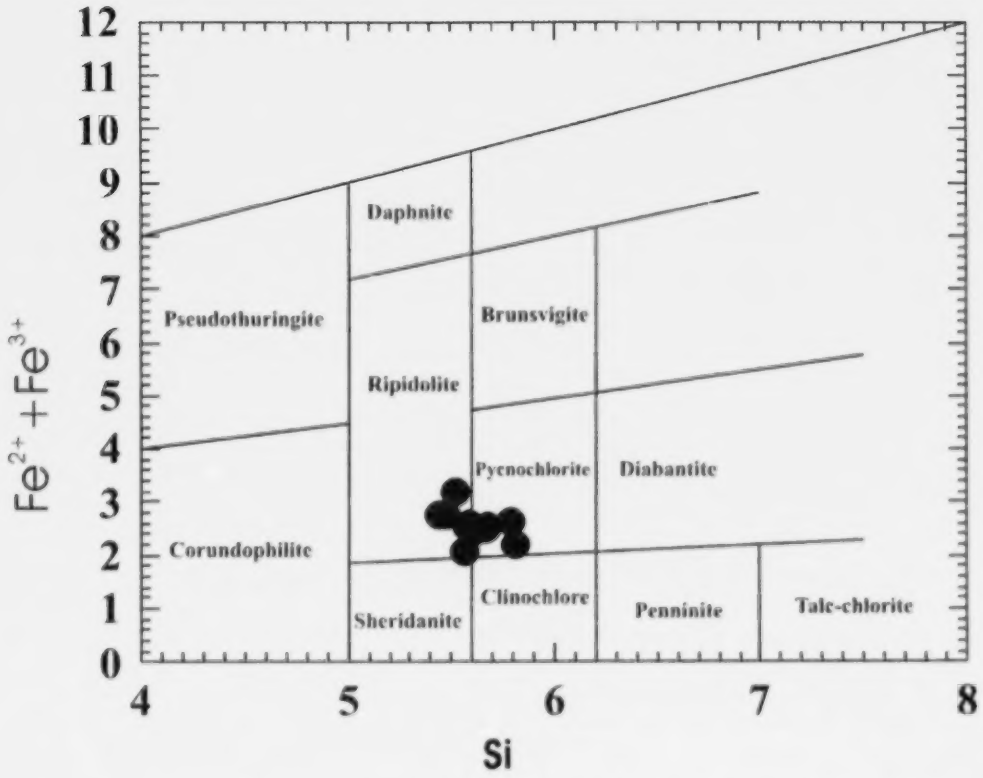


**Figure 8:** Composition of chlorite. Nomenclature of chlorite is after Deer, Howie and Zussman (1972).

# Rock Chemistry

Eleven samples representing an ultramafic xenolith, breccia matrix, breccia (matrix+xenoliths), lamprophyre dikes and diabase were collected for whole rock chemical analyses. The analyses were done at the Geoscience Laboratories, Geoservices Centre in Sudbury using the methods of analysis and detection limits listed with the results in Table 8.

The samples show considerable variation in abundance of major elements. In view of the compositional variation and the interpretation by some workers that the breccias represent volcanic rocks, the volcanic classification scheme of Jensen (1976) is used for comparative purposes. The magnesium-rich ultramafic xenolith (Mg#=84) plots within the komatiitic field (Figure 9a). Samples of breccia matrix from the Engagement and Cristal occurrences (Mg#=78 to 80) are tightly clustered near the boundary between fields of komatiite and basaltic komatiite. The breccia (breccia matrix+xenoliths) and lamprophyre dikes have lower Mg#s (60 to 75) and somewhat overlapping compositions variable between fields of basaltic komatiite and high-magnesium tholeiite. The FeO- and $TiO_2$-rich diabase (Mg#=34) is compositionally unique and plots within the field of high-iron tholeiite.

**Table 8:** Rock chemistry.

| Sample | Method | Detection | 02DS86 | 02DS87 | 02DS88 | 02DS89 | 02DS90 | 02DS92 | 02DS94 | 02DS96 | 02DS97 | 02DS98 | 02DS99 |
|---|---|---|---|---|---|---|---|---|---|---|---|---|---|
| Rock Type | | Limit | 1 | 1 | 2 | 1 | 2 | 4 | 2 or 3 | 1 or 3 | 5 | 3 | 3 |
| Area | | | Engage-ment Zone | Engage-ment Zone | Engage-ment Zone | Cristal | Cristal | Barnet Lake Zone | Heterolithic Breccia | Heterolithic Breccia | Fine grained dike | Sandor dike | Xenolith-rich dike |
| Easting | | | 667729 | 667729 | 667729 | 666482 | 666482 | 665570 | 656724 | 656022 | 656022 | 659967 | 658000 |
| Northing | | | 5336050 | 5336050 | 5336050 | 5337338 | 5337338 | 5333068 | 5340156 | 5340393 | 5340393 | 5342068 | 5344000 |
| SiO2 | WD-XRF | 0.01 (wt%) | 45.28 | 44.58 | 48.88 | 45.26 | 51.52 | 52.1 | 52.21 | 44.42 | 52.52 | 47.12 | 47.91 |
| Al2O3 | WD-XRF | 0.01 | 8.56 | 8.88 | 10.83 | 8.58 | 13.92 | 3.09 | 10.66 | 11.23 | 13.45 | 11.14 | 11.24 |
| MnO | WD-XRF | 0.01 | 0.16 | 0.16 | 0.17 | 0.16 | 0.19 | 0.18 | 0.13 | 0.14 | 0.23 | 0.15 | 0.15 |
| MgO | WD-XRF | 0.01 | 18.8 | 19.42 | 12.71 | 20.67 | 8.8 | 21.36 | 13.15 | 9.24 | 4.2 | 11.46 | 11.64 |
| CaO | WD-XRF | 0.01 | 9.58 | 9.72 | 8.47 | 9.33 | 6.2 | 12.39 | 6.81 | 7.58 | 8.29 | 7.98 | 8.57 |
| Na2O | WD-XRF | 0.01 | 1.04 | 0.88 | 2.4 | 0.31 | 4.18 | 0.2 | 3.4 | 2.51 | 2.44 | 2.44 | 3.38 |
| K2O | WD-XRF | 0.01 | 0.26 | 0.22 | 1.17 | 0.2 | 1.22 | 0.37 | 1.55 | 3.93 | 0.99 | 3.43 | 2.25 |
| TiO2 | WD-XRF | 0.01 | 0.7 | 0.69 | 0.82 | 0.72 | 1.1 | 0.06 | 0.66 | 0.81 | 1.83 | 0.89 | 1 |
| P2O5 | WD-XRF | 0.01 | 0.31 | 0.31 | 0.22 | 0.31 | 0.13 | N.D. | 0.23 | 0.33 | 0.18 | 0.42 | 0.35 |
| Fe2O3T | WD-XRF | 0.01 | 10.5 | 10.5 | 10.73 | 10.32 | 11.6 | 8.33 | 8.81 | 9.66 | 16.45 | 11.96 | 10.44 |
| LOI | WD-XRF | 0.01 | 4.84 | 5.38 | 3.36 | 4.86 | 2.58 | 3.04 | 1.72 | 10.17 | 0.54 | 2.22 | 2.31 |
| Total | | | 100.03 | 100.75 | 99.78 | 100.73 | 101.45 | 101.11 | 99.34 | 100.01 | 101.14 | 99.22 | 99.26 |
| CO2 | IR Spectr. | 0.03 | 0.94 | 1.11 | 0.66 | 0.13 | 0.41 | 0.83 | 0.09 | 8.75 | 0.76 | 1.06 | 1.97 |
| S | IR Spectr. | 0.01 | 0.05 | 0.01 | N.D. | 0.01 | 0.01 | N.D. | N.D. | 0.08 | 0.15 | 0.01 | 0.03 |
| Rb | ICP-MS | 0.01 (ppm) | 8.68 | 7.03 | 30.48 | 2.75 | 33.18 | 13.52 | 52.92 | 164.79 | 40.51 | 145.67 | 80.58 |
| Ba | ICP-MS | | 63 | 30 | 668 | 253 | 495 | 100 | 398 | 1845 | 356 | 746 | 1109 |
| Sr | ICP-MS | 0.2 | 153.87 | 166.9 | 360.49 | 81.93 | 402.33 | 59 | 542 | 466 | 176.11 | 422.09 | 824 |
| Ce | ICP-MS | 0.01 | 1.16 | 1 | 2.96 | 0.33 | 3.53 | 0.84 | 2.85 | >5.00 | 1.67 | >5.00 | 4.5 |
| Be | ICP-OES | 3 | N.D. | N.D. | N.D. | N.D. | N.D. | N.D. | N.D. | N.D. | N.D. | N.D. | N.D. |
| Mo | ICP-OES | 5 | N.D. | N.D. | N.D. | N.D. | N.D. | N.D. | N.D. | N.D. | N.D. | N.D. | N.D. |
| Ta | ICP-MS | 0.01 | N.D. | N.D. | N.D. | N.D. | N.D. | N.D. | 0.34 | N.D. | 1 | N.D. | 0.4 |
| Hf | ICP-MS | 0.01 | 1.9 | 1.76 | 2.15 | 2.29 | 2.2 | N.D. | 2.78 | 2.14 | 4.72 | 2.35 | 2.42 |
| Ga | ICP-MS | | 12 | 13 | 13 | 12 | 15 | 6 | 14 | 14 | 22 | 16 | 15 |
| Nb | ICP-MS | 0.02 | 4.03 | 4.17 | 3.32 | 3.96 | 3.94 | N.D. | 4.88 | 3.9 | 16.99 | 4.89 | 7.61 |
| Sn | | | N.D. | N.D. | N.D. | N.D. | N.D. | N.D. | N.D. | N.D. | N.D. | N.D. | 5 |
| Zr | WD-XRF | 1 | 63 | 63 | 83 | 81 | 88 | 4 | 120 | 91 | 160 | 96 | 118 |
| Zr | ICP-MS | | 65.88 | 65.56 | 79.08 | 86.97 | 85.79 | N.D. | 112.82 | 85.34 | 168.75 | 88.79 | 98.68 |
| Co | ICP-OES | 5 | 75 | 76 | 66 | 75 | 64 | 59 | 55 | 55 | 65 | 61 | 60 |
| Cr | WD-XRF | 2 | 1292 | 1350 | 765 | 1369 | 490 | 2348 | 858 | 541 | 53 | 720 | 633 |
| Cu | ICP-OES | 5 | 566 | N.D. | 66 | 25 | 75 | N.D. | 13 | 41 | 105 | 18 | 83 |
| Ni | ICP-OES | 5 | 790 | 795 | 420 | 781 | 256 | 1526 | 495 | 302 | 49 | 371 | 365 |
| V | ICP-OES | 5 | 160 | 154 | 193 | 139 | 251 | 57 | 129 | 180 | 383 | 213 | 176 |
| Zn | ICP-OES | 2 | 99 | 102 | 100 | 106 | 86 | 115 | 83 | 100 | 135 | 99 | 106 |
| Pb | WD-XRF | 7 | 8 | 7 | 8 | 5 | 8 | 8 | 10 | 10 | 12 | 10 | 10 |
| Th | ICP-MS | 0.02 | 1.81 | 1.75 | 1.65 | 3.09 | 1.35 | N.D. | 3.47 | 3.29 | 4.48 | 3.2 | 3.97 |
| U | ICP-MS | 0.02 | 0.43 | 0.37 | 0.42 | 0.38 | 0.33 | 0.02 | 0.84 | 0.96 | 1.19 | 0.79 | 0.77 |
| | | 0 | | | | | | | | | | | |
| Sc | ICP-OES | 1 | 21 | 21 | 28 | 20 | 34 | 4 | 18 | 24 | 39 | 27 | 25 |
| Y | ICP-MS | 2 | 15.03 | 14.53 | 18.93 | 13.6 | 22.54 | 1.07 | 15.99 | 17.45 | 40.42 | 20.16 | 18.21 |
| Sample | | | | | | | | | | | | | |
| La | ICP-MS | 0.01 | 15.46 | 14.53 | 13.31 | 14.47 | 9.8 | 0.52 | 23.34 | 18.5 | 22.44 | 18.7 | 23.5 |
| Ce | ICP-MS | 0.01 | 33.74 | 32.58 | 29.29 | 33.78 | 22.46 | 0.86 | 49.67 | 39.92 | 47.62 | 40.57 | 52.95 |
| Pr | ICP-MS | 0.01 | 4.46 | 4.29 | 3.97 | 4.45 | 3.04 | 0.11 | 6.25 | 5.21 | 6.12 | 5.39 | 7.34 |
| Nd | ICP-MS | 0.01 | 19.1 | 17.76 | 17.17 | 18.51 | 14.09 | 0.66 | 25.02 | 22.41 | 25.32 | 23.1 | 31.75 |
| Sm | ICP-MS | 0.01 | 3.78 | 3.84 | 3.88 | 4.06 | 3.43 | 0.19 | 4.66 | 5.09 | 6.35 | 5.06 | 6.37 |
| Eu | ICP-MS | 0.01 | 1.17 | 1.13 | 1.36 | 1.19 | 1.31 | 0.06 | 1.41 | 1.64 | 2.01 | 1.74 | 1.94 |
| Gd | ICP-MS | 0.01 | 3.37 | 3.24 | 3.76 | 3.46 | 3.74 | 0.18 | 3.84 | 4.45 | 6.9 | 4.64 | 5.11 |
| Tb | ICP-MS | 0.01 | 0.48 | 0.44 | 0.58 | 0.47 | 0.65 | 0.02 | 0.54 | 0.58 | 1.11 | 0.65 | 0.65 |
| Dy | ICP-MS | 0.01 | 2.76 | 2.52 | 3.3 | 2.6 | 3.87 | 0.14 | 2.83 | 3.12 | 7.13 | 3.69 | 3.47 |
| Ho | ICP-MS | 0.01 | 0.57 | 0.56 | 0.69 | 0.52 | 0.86 | 0.03 | 0.57 | 0.63 | 1.54 | 0.74 | 0.66 |
| Er | ICP-MS | 0.01 | 1.49 | 1.5 | 1.96 | 1.36 | 2.5 | 0.11 | 1.56 | 1.75 | 4.45 | 1.93 | 1.7 |
| Tm | ICP-MS | 0.01 | 0.23 | 0.22 | 0.29 | 0.18 | 0.36 | 0.02 | 0.22 | 0.27 | 0.65 | 0.29 | 0.25 |
| Yb | ICP-MS | 0.01 | 1.42 | 1.33 | 1.9 | 1.25 | 2.41 | 0.12 | 1.47 | 1.59 | 4.31 | 1.77 | 1.43 |
| Lu | ICP-MS | 0.01 | 0.209 | 0.197 | 0.287 | 0.176 | 0.358 | 0.032 | 0.212 | 0.245 | 0.635 | 0.271 | 0.225 |
| Total | | | 88.259 | 84.137 | 81.747 | 86.476 | 68.878 | 2.852 | 121.592 | 105.405 | 136.585 | 108.541 | 137.345 |
| $La/Yb_{NC1\ Chondrite}$ | | | 8 | 8 | 5 | 8 | 3 | 3 | 11 | 8 | 4 | 8 | 12 |
| Mg# | | | 78 | 79 | 70 | 80 | 60 | 84 | 75 | 65 | 34 | 66 | 69 |

**Rock Type Codes**

1 Breccia matrix
2 Breccia
3 Lamprophyre dike
4 tremolitic inclusion
5 Diabase dike

WD-XRF wavelength dispersive X-ray fluorescence
IR Spectr Spectroscopy
ICP-OES inductively coupled plasma optical emission spectroscopy
ICP-MS inductively coupled plasma mass spectroscopy

N.D. not detected

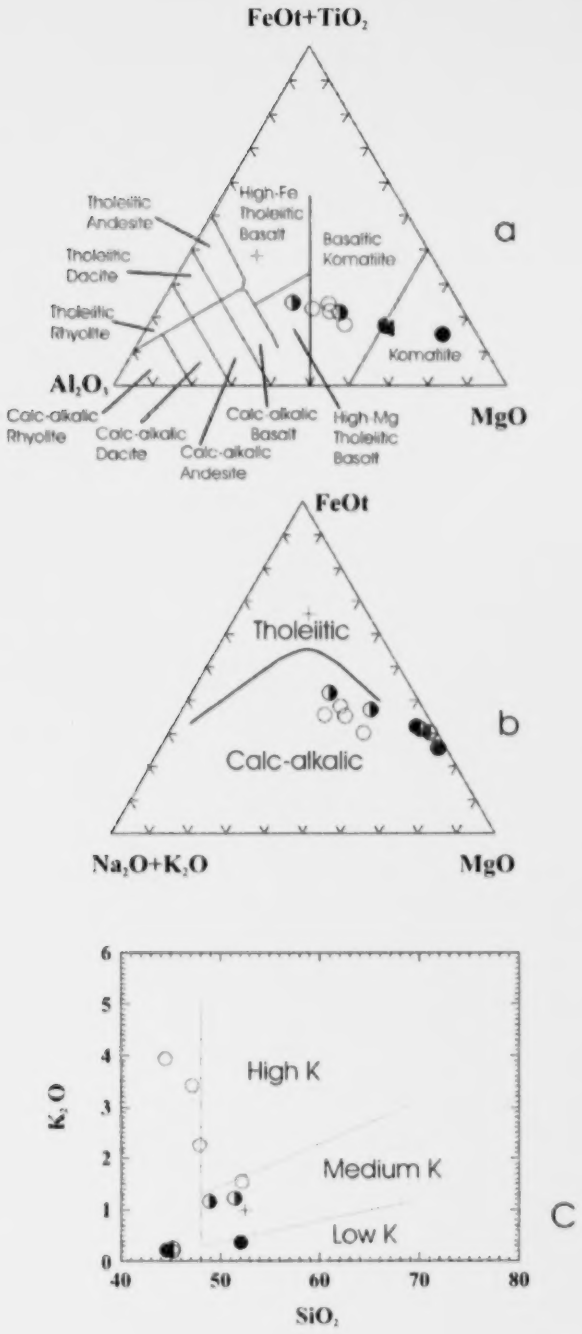


**Figure 9**: Major element characteristics: (a) cation plot of Jensen (1976); (b) calc-alkalic-tholeiite plot of Irving and Baragar (1971); (c) alkalinity plot of Le Maitre (1989). Symbols are: solid circle = ultramafic xenolith; left-filled circle = breccia matrix from the Engagement and Cristal occurrences; right-filled circle = breccia from the Engagement and Cristal occurrences; open circle = lamprophyre dikes and breccia from the Oasis occurrence; cross = diabase dike.

The ultramafic xenolith and breccia matrix have low alkaline elements and similar FeO/MgO ratios and plot within a cluster along the FeO-MgO join on the discrimination diagram of Irving and Baragar (1971; Figure 9b). Samples of breccia (breccia matrix+xenoliths) and lamprophyre dikes are enriched in $Na_2O+K_2O$ and slightly enriched in FeO compared to breccia matrix and are calc-alkalic. The diabase is strongly FeO-enriched and plots within the tholeiitic field.

Although many samples have an $SiO_2$ content that is too low for accurate classification using the $K_2O$-$SiO_2$ systematics of Le Maitre (1989), the ultramafic xenolith and breccia matrix samples have less than 1 wt.% $K_2O$ and are compatible with low-potassium volcanic rocks (Figure 9c). Samples of the breccia, lamprophyre dikes and the diabase dike, have 1 to 4 wt.% $K_2O$ and, in this respect, are similar to medium- or high-potassium volcanic rocks.

Rare-earth elements (REE) in the ultramafic xenolith vary from 0.5 to 1.5 times chondritic values and show a somewhat irregular and overall concave downward profile (Figure 10a) with the greatest depletion in Ce, Pr and heavy rare earth elements (HREE) except Lu. Sage (2000b) reported geochemical analyses of a larger set of xenoliths from lamprophyre dikes. The REE profiles of these samples generally have flat HREE at 0.2 to 3.0 times chondrite whereas light rare earth elements (LREE) are variably enriched from 4 to 100 times chondrite. The combined data of Sage (2000b) and this study show considerable compositional variation in the ultramafic xenoliths. Although the REE variation can be due to local mobilization of REEs during alteration (Menard et al. 1999) it probably also reflects primary compositional variation in the xenoliths.

The REE concentrations are greater in other rocks than in the xenolith. REE for breccia and dike samples vary from 7 to 100 times chondritic values and are sloped from left to right (*see* Figure 10a). Samples of breccia matrix from the Engagement and Cristal occurrences have consistent $La/Yb_N$ values of 8 and smooth, sloped profiles. In contrast, the breccia samples from the same occurrences have lower $La/Yb_N$ values (3 to 5) with slight positive Eu anomalies. The breccia is more enriched in HREE and depleted in LREE than breccia matrix with the result that REE profiles for the breccia matrix and breccia samples cross each other. The lower slope of REE profiles for breccia samples can be explained by the compositional changes that result from mixing volcanic xenoliths with breccia matrix. Sub-equal volumes of volcanic xenoliths with fairly flat REE profiles at 20 to 30 times chondrite values and breccia matrix with moderately sloped profiles ($La/Yb_N$=8) could produce the weakly sloped profiles characteristic of breccia.

The lamprophyre dikes and breccia samples from the Oasis occurrence have greater REE-enrichment and more steeply sloped REE profiles ($La/Yb_N$=8 to 12) than the breccia matrix at the Engagement and Cristal occurrences (compare Figures 10a and 10b). This confirms earlier observations based on mineral chemistry and petrography that rocks interpreted as breccia at the Oasis occurrence are more akin to lamprophyre dikes than to breccia at the Engagement and Cristal occurrences.

The diabase dike is compositionally distinct from other rocks. It is enriched in HREE at 20 to 30 times chondrite and has a slightly sloped REE profile with $La/Yb_N$=4.

Many trace elements are below detection limit in the ultramafic xenolith (Table 8) and preclude accurate definition of trace element profiles. Nonetheless, the available primitive mantle-normalized trace elements in the ultramafic xenolith (mainly REE) are consistently less than 1 (Figure 10c) with the greatest depletion in Ce, Pr and HREE.

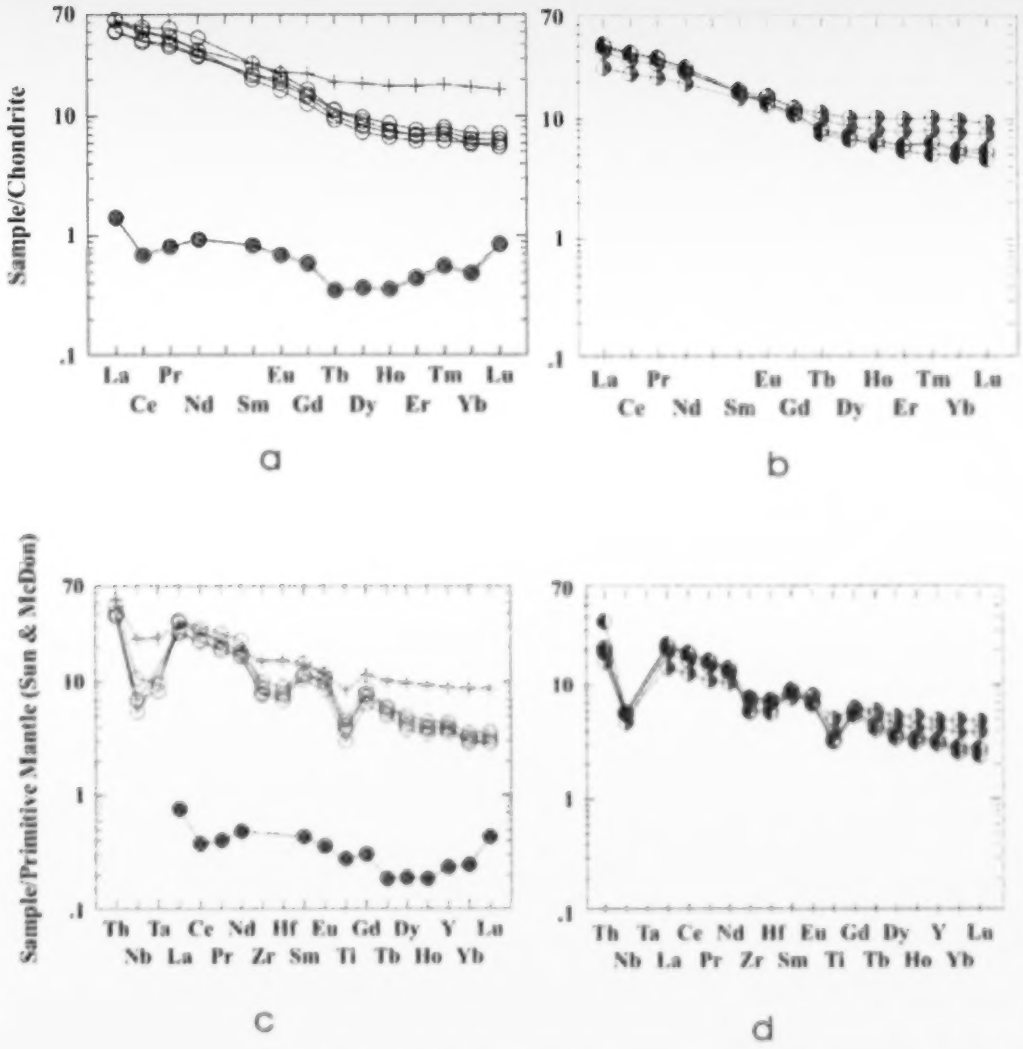


**Figure 10**: Trace element characteristics: (a and b) chondrite-normalized rare earth element profiles; (c and d) primitive mantle normalized trace element profiles. Normalizing values are from Sun and McDonough (1989). Symbols are: solid circle = ultramafic xenolith; left-filled circle = breccia matrix from the Engagement and Cristal occurrences; right-filled circle = breccia from the Engagement and Cristal occurrences; open circle = lamprophyre dikes and breccia from the Oasis occurrence; cross = diabase dike.

Primitive mantle-normalized trace element profiles for various breccia and dike samples are enriched from 2 to 50 times primitive mantle and are sloped from left to right due to greater enrichment in incompatible elements relative to compatible elements. The profiles show deep troughs corresponding to Nb, Ta, Zr, Hf, and Ti. Samples of breccia matrix from the Engagement and Cristal occurrences generally show the least overall enrichment although the mixing of volcanic xenoliths with breccia matrix causes the slope of breccia profiles to be more shallow than the slope of breccia matrix profiles. Breccia is more enriched in compatible elements and less enriched in incompatible elements than breccia matrix.

The trace element profiles of lamprophyre dikes and breccia from the Oasis occurrence are parallel to those of breccia matrix but are somewhat more enriched in all elements and accordingly, plot higher on the graph (compare Figures 10c and 10d). The diabase dike shows the greatest enrichment in trace elements except LREE.

Williams (2002) reported geochemistry of Wawa lamprophyre dikes that is similar to the results of this study. The primitive mantle-normalized trace element profiles of Williams (2002) are enriched from 2 to 100 times primitive mantle values with the greatest enrichment in incompatible elements and troughs corresponding to Nb, Zr, Hf, and Ti. Using data of Rock (1991) and Mitchell (1995), Williams (2002) noted that the Wawa lamprophyres are less enriched in REE and most trace elements, particularly incompatible elements (Th, U, Nb, LREE, P, Nb, Zr and Hf) than the average minette, spessartite and Archean calc-alkalic lamprophyre. Williams (2002) went on to compare the chemistry of diamondiferous and non-diamondiferous lamprophyres at Wawa and noted that the diamondiferous varieties tend to be more primitive. Diamondiferous lamprophyres have high Mg#s and have the least enrichment in high field strength elements (Zr, Hf, Nb, Ta), large ion lithophile elements (Rb, Sr, Ba, U and Th) and REE. Broadly, the primitive mantle-normalized trace element profiles of the breccia matrix and lamprophyres including progressive enrichment in incompatible elements with troughs corresponding to Nb, Ta and Ti are consistent with magmas erupted in volcanic arcs (Pearce 1996).

# Metamorphism

Rock (1991) noted that fresh calc-alkalic spessartites have a mineral assemblage of amphibole+biotite +clinopyroxene+feldspars+feldspathoids+olivine+quartz. These primary minerals are extensively altered under late-stage subsolidus conditions due to the high volatile content of lamprophyres with the result that secondary carbonates, chlorite, epidote, serpentine and zeolites are commonly as abundant as the magmatic phases. Wyman and Kerrich (1993) noted that calcite and albite occur widely in lamprophyre dikes of the Abitibi greenstone belt.

Lamprophyre dikes and breccias of the Wawa area are extremely altered or metamorphosed in comparison with other lamprophyres. Although primary minerals such as pyroxene and chromite are identified (Sage 2000b), these are rare. Aluminous amphiboles of presumably primary origin are identified fairly widely in samples of this study although they are largely converted to actinolite and chlorite. Most samples have an assemblage of actinolite+chlorite+albite±epidote±calcite±quartz with accessory titanite (Table 2), which provides insight on the pressure-temperature conditions of metamorphism.

Within mafic rocks, the assemblage actinolite+chlorite+epidote+quartz is diagnostic of the upper greenschist facies (Liou, Kuniyoshi and Ito, 1974; Moody, Meyer and Jenkins, 1983) and has an upper limit of 475°C at 2 kbars (Liou, Kuniyoshi and Ito, 1974). Schiffman and Liou (1980) indicate that the mineral assemblage prehnite+chlorite+actinolite±quartz±albite is stable between 2.5 and 5 kbars at temperatures of 325° to 375°C. This represents an intermediate stage between the sub-greenschist assemblage pumpellyite+chlorite+actinolite and the upper greenschist facies assemblage (above) for mafic rocks (Figure 11). Although pressure is poorly constrained at the time that breccia zones and lamprophyre dikes were emplaced, the pressure is likely low (<5 kbars) based on comparison with crystallization pressures for late Archean plutonic rocks through large areas of the western Superior Province (Stone 2000 and unpublished data). This, combined with the lack of prehnite and pumpellyite, indicates that the alteration or metamorphism of the breccias and lamprophyres occurred at upper greenschist conditions corresponding to temperatures of 375° to 475°C (*see* Figure 11).

Lamprophyres and breccias of the Wawa area show widespread development of a foliation and are locally folded and faulted. Although late-stage alteration is endemic to lamprophyres, the degree of alteration and P-T conditions of alteration appear to be uniform through the study area. These observations and the available geochronology are consistent with the interpretation that the lamprophyres and breccia zones were affected by regional deformation and metamorphism. In Archean terranes, regional deformation normally precedes episodes of pluton emplacement with accompanying metamorphism (Easton 2000). At Wawa, lamprophyres with known ages in the range 2685 to 2674 Ma were emplaced at approximately the same time as post 2682 Ma sedimentation events (Corfu and Sage 1992). The sedimentary sequences were affected by regional folding and faulting (Arias and Helmstaedt 1990) followed by a major period of plutonism at 2686 to 2662 Ma (Turek, Sage and Van Schmus 1992). Although not directly dated, metamorphism is likely to have accompanied the late plutonic event and hence, affected the lamprophyres and breccia zones.

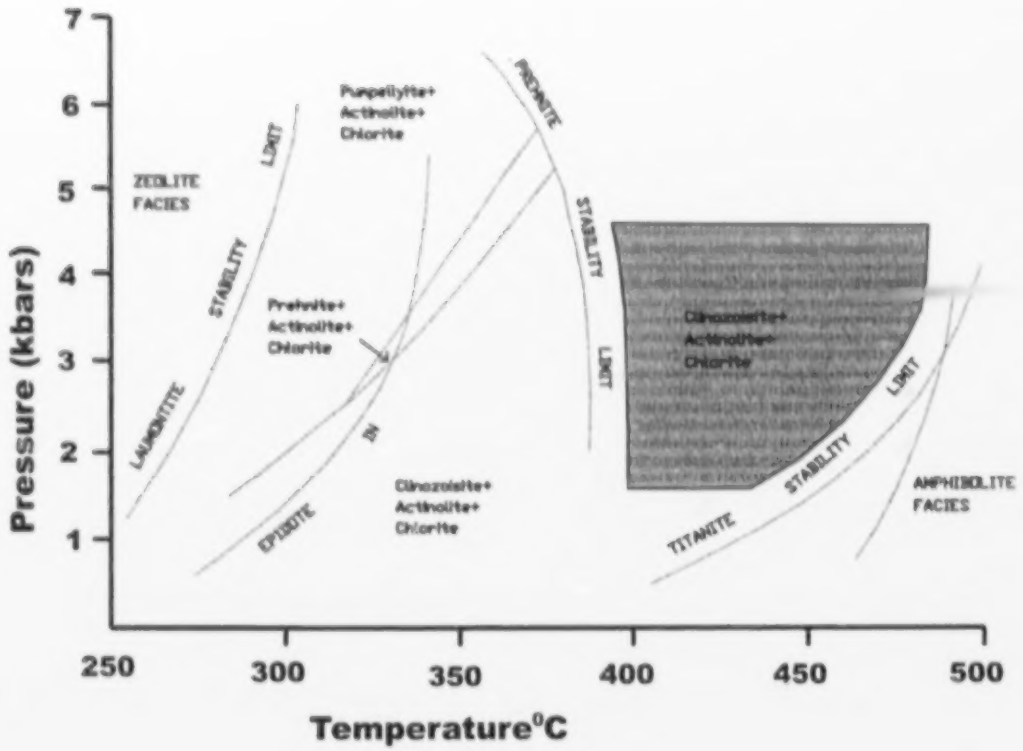


**Figure 11:** Pressure-temperature plot showing the stability fields of index minerals and assemblages. The shaded area shows the estimated P-T conditions under which breccia and lamprophyre dikes were metamorphosed. Epidote and titanite stability fields are from Moody, Meyer and Jenkins (1983); greenschist-amphibole facies boundary is from Liou, Kunoyoshi and Ito (1974). Phase relations between actinolite, chlorite, clinozoisite and pumpellyite are from Schiffman and Liou (1980).

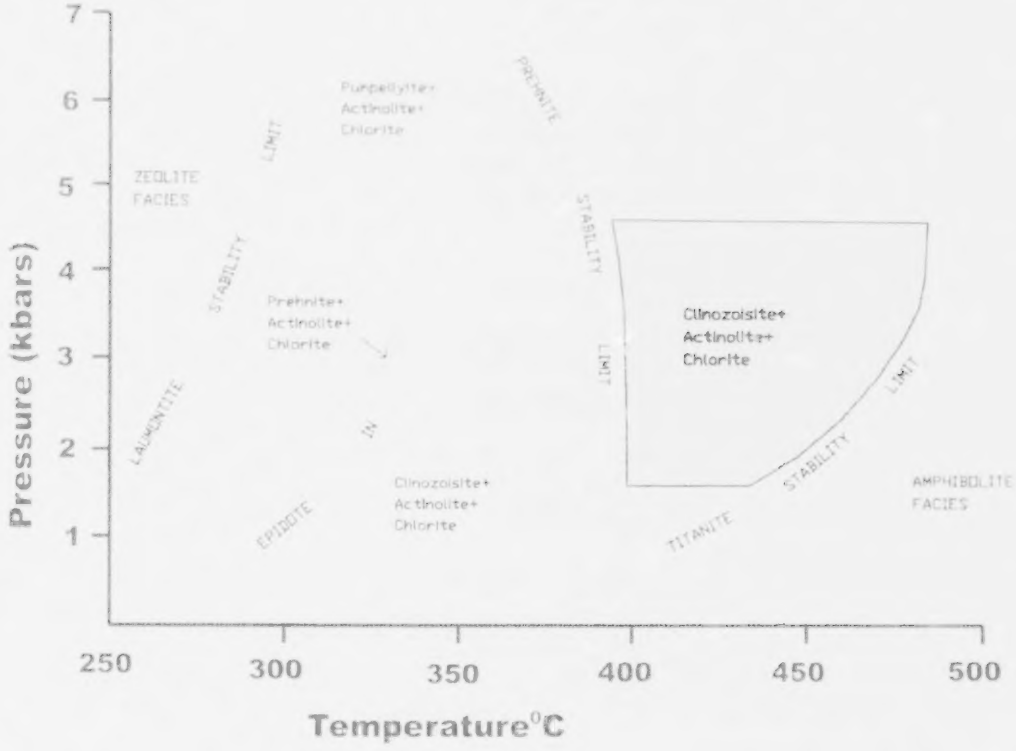


**Figure 11:** Pressure-temperature plot showing the stability fields of index minerals and assemblages. The shaded area shows the estimated P-T conditions under which breccia and lamprophyre dikes were metamorphosed. Epidote and titanite stability fields are from Moody, Meyer and Jenkins (1983); greenschist-amphibolite facies boundary is from Liou, Kumovoshi and Ito (1974). Phase relations between actinolite, chlorite, clinozoisite and pumpellyite are from Schiffman and Liou (1980).

# Heavy Mineral and Diamond Processing

Two samples of breccia matrix (02DS86 and 02DS87) were collected from the Engagement occurrence for analysis of heavy minerals. At the Geoscience Laboratories, Geoservices Centre in Sudbury, the fissile samples were broken into fist-sized pieces using a hammer and the material was subsequently passed through a jaw crusher and reduced to <1 mm size using a Fritsch disk mill. The samples were then dry-screened followed by wet screening using a Fritsch sieve shaker with screen sizes of 0.6, 0.25 and 0.068 mm. The <0.068 mm fraction was dried and archived. Magnetic separation using a Carpco magnetic separator was completed on parts of the 0.6-1.0, 0.25-0.60 and 0.068-0.25 mm size fractions (Table 9). The magnetic separation generally succeeded in removing more than 95% of the weakly magnetic silicate minerals (mainly actinolite). The non-magnetic fractions of 02DS86 were immersed in methylene iodide (density of 3.25), which effectively floated off the remaining light minerals and produced a heavy mineral concentrate weighing typically less than 1 gm (*see* Table 9). The mineral assemblage of the heavy concentrates for the coarser fractions of 02DS86 was determined by examining the grains with a Leica Wild M10 stereoscope and a Volpi Intralux 6000 halogen light source.

Sample 02DS87 was processed by the same procedure as 02DS86 and produced small non-magnetic fractions and very small heavy mineral concentrates (*see* Table 9) dominated by zircon. No diamonds were observed in the heavy mineral concentrate.

The heavy mineral concentrates of the coarser fractions of 02DS86 are characterized by a mineral assemblage of pyrite+rutile+zircon+titanite with accessory diamond (*see* Table 9). Diamonds were picked from the heavy concentrates on the basis of their crystal form, colour, luster and surface texture. Each grain was analyzed using an energy dispersive (ED) detector of the JEOL 6400 scanning electron microscope (SEM). Although carbon is below the detection limit for ED, the SEM analysis showed that the grains contained no elements heavier than carbon. Hence, it is concluded on the basis of their appearance and the SEM analysis that the grains are composed of carbon and represent diamond.

Secondary electron micrographs were taken of selected diamonds using an accelerating voltage of 25 kV and a beam current of 0.07 nA. The micrographs effectively display the morphology and surface texture of the diamonds (Figure 12) whereas a stereoscope was used to record colour of the grains.

**Table 9:** Diamond processing. HMC = heavy mineral concentrate.

| Sample (weight kg) | Carpco Feed grain size (mm) | weight (gm) | Non-mag heavy liquid feed (gm) | HMC weight (gm) | HMC mineral assemblage | No. of diamonds |
|---|---|---|---|---|---|---|
| 02DS86 (48 kg) | >0.6 | 6338 | | 0.1178 | pyrite, rutile, zircon, titanite | 8 |
| | 0.6 to 0.25 | 3204 | 70.8603 | 0.1545 | pyrite, rutile, zircon, titanite | 49 |
| | 0.25 to 0.068 | 1738 | 40.4851 | 0.4438 | too fine to pick, diamonds present | |
| | <0.068 | not processed | | | | |
| 02DS87 (60 kg) | >0.6 | 4564 | 258.0517 | 0.0042 | pyrite, titanite | 0 |
| | 0.6 to 0.25 | 2228 | 15.4572 | 0.005 | zircon, pyrite, titanite | 0 |
| | 0.25 to 0.068 | 2022 | 35.3186 | 0.007 | zircon, pyrite | 0 |
| | <0.068 | not processed | | | | |

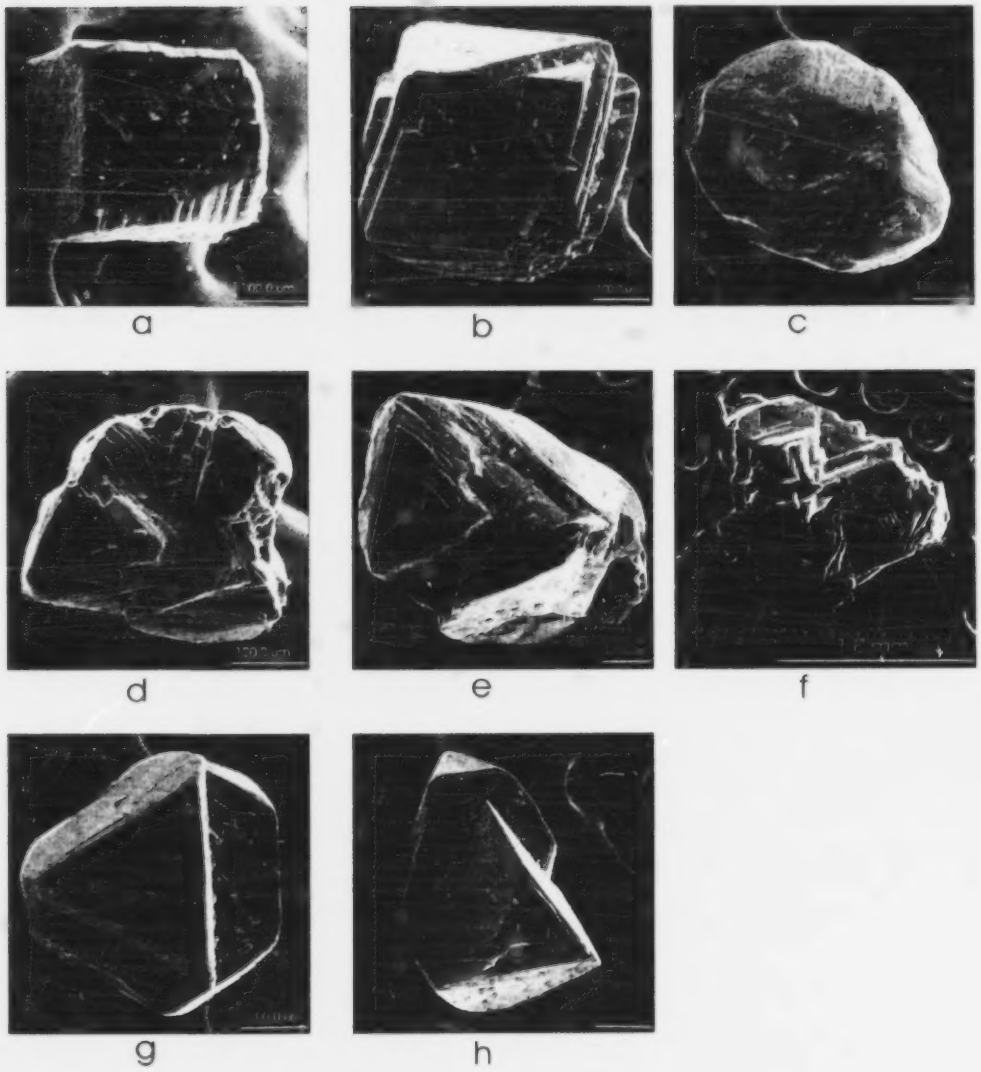


**Figure 12**: Selected diamond grains from the Engagement occurrence: (a) equidimensional cube with flat, corroded surfaces and yellow colour. (b) An equidimensional octahedral twin with a primary morphology characterized by stepwise lamellar surfaces. The grain has a yellow tinge. (c) An equidimensional octahedral grain modified to a dodecahedroid with a hackly surface by resorption. The grain is clear and colourless. (d) A complex, broken aggregate showing polycentric and stepwise lamellar surfaces. (e) A broken crystal of unknown habit and primary morphology and polycentric/imbricated surface texture. The grain is clear and colourless. (f) A broken grain of unknown habit with stepwise lamellar and polycentric surface texture. The grain is clear and colourless. (g) An equidimensional macle with primary morphology and flat surface texture. The grain is chipped and has a smokey colour. (h) A complex twin with flat surface texture (minimal stepwise lamellae). The crystal is clear and broken.

## DIAMOND CHARACTERISTICS

A total of 57 diamonds were separated from approximately 9.5 kg of material representing sample 02DS86. Of these, 8 grains were derived from the greater than 0.60 mm fraction whereas 49 were separated from the 0.06-0.25 mm fraction. Of the entire population, 11% of the diamonds are whole, 70% are broken and 18% are chipped. Broken grains have surfaces defined by fractures comparable in size to the diameter of the grain. A chip is a missing fragment of a grain that is small in comparison with the diameter of the grain. Although individual grains could not be accurately weighed or measured, it was observed that the broken grains comprise the largest member of the grain population. It is unclear whether the breakage occurred during laboratory processing of the sample or by earlier geologic processes.

No assessment of diamond price or value was completed on the grains as none was above the recommended size of 0.85 mm as outlined in Guidelines for Reporting of Diamond Exploration Results (Canadian Institute of Mining and Metallurgy, March 2003). The characteristics of whole, chipped and broken grains are described separately in Table 10 using descriptive criteria of Otter, McCallum and Gurney (1991) and McCallum et al. (1991).

## MORPHOLOGY AND COLOUR OF DIAMOND GRAINS

Although equidimensional diamond grains are prevalent (*see* Figures 12a, b, g, h), other shapes including distorted, flattened, complex and unknown are well represented in the populations (*see* Table 10). The primary morphology of diamond grains is classified mainly as octahedral (*see* Figure 12b) and aggregate crystal forms (*see* Figures 12d, f) although approximately a third of the grains are of unknown form. Cube, macle and complex twin forms make up minor components of the grain population. Apices are commonly very sharp on octahedral and twinned crystals and the majority of the crystals exhibit only primary morphology with limited resorption. Highly resorbed crystals account for only 7% of the diamond population (*see* Figure 12c).

The majority of diamonds are colourless (61%) although yellow grains, occurring as octahedrons and cubes, account for 14% of the population. Smokey brown grains account for 23% of the population and are represented by all crystal forms including resorbed dodecahedroids. No inclusions could be observed in the grains.

Flat surfaces have been observed on 14% of the diamond population (*see* Figure 12g). Growth layers, represented by stepwise lamellar development of faces (*see* Figure 12d, e, and f) occur commonly (50% of the population) on the primary crystals. Polycentric crystals (*see* Figure 12d) are also common.

**Table 10:** Crystal regularity, morphology, surface textures, dissolution features and colour of diamond grains.

Crystal Regularity

| | equidim | distort | flattened | complex | unknown | total |
|---|---|---|---|---|---|---|
| entire population[1] | *27%* | *14%* | *14%* | *23%* | *21%* | 100% |
| whole crystals | 40% | 20% | 20% | 10% | 10% | 100% |
| chipped crystals | 50% | 17% | 0% | 33% | 0% | 100% |
| broken crystals | 21% | 10% | 15% | 26% | 28% | 100% |

Primary Morphology

| | octahedra | cubo-octa | cube | aggregate | macle[2] | other twin | unknown | total |
|---|---|---|---|---|---|---|---|---|
| entire population[1] | *23%* | *0%* | *2%* | *27%* | *4%* | *13%* | *32%* | 100% |
| whole crystals | 60% | 0% | 0% | 0% | 0% | 20% | 20% | 100% |
| chipped crystals | 17% | 0% | 17% | 33% | 0% | 33% | 0% | 100% |
| broken crystals | 15% | 0% | 0% | 33% | 5% | 8% | 38% | 100% |

Secondary Morphology (resorption)

| | primary (5) | remnant (3) | dodecahedroids (1) | total |
|---|---|---|---|---|
| Population | *84%* | *9%* | *7%* | *100%* |
| whole crystals | 50% | 30% | 20% | 100% |
| chipped crystals | 83% | 0% | 17% | 100% |
| broken crystals | 95% | 3% | 3% | 100% |

Colour

| | colourless | yellow | smokey | total |
|---|---|---|---|---|
| entire population[1] | *61%* | *14%* | *23%* | *98%* |
| whole crystals | 70% | 20% | 10% | 100% |
| chipped crystals | 33% | 50% | 17% | 100% |
| broken crystals | 63% | 8% | 28% | 99% |

Surface Texture

| | flat | stepwise lamellar | imbricated | polycentric |
|---|---|---|---|---|
| entire population[1] | *14%* | *50%* | *18%* | *32%* |
| whole crystals | 20% | 70% | 10% | 20% |
| chipped crystals | 17% | 83% | 0% | 17% |
| broken crystals | 13% | 49% | 23% | 38% |

Dissolution Features

| | hackly | growth | droplet | trignol etch | grooved | corroded | block |
|---|---|---|---|---|---|---|---|
| entire population[1] | *4%* | *2%* | *0%* | *5%* | *9%* | *2%* | *0%* |
| whole crystals | 20% | 0% | 0% | 10% | 20% | 0% | 0% |
| chipped crystals | 0% | 0% | 0% | 17% | 0% | 17% | 0% |
| broken crystals | 0% | 3% | 0% | 3% | 5% | 0% | 0% |

[1] calculated from raw data, if weighted mean calculated from percentage crystal fracture and characteristic, rounding error will occur. For example crystal regularity for entire population = 28% if calculated 0.4 x 11% + 0.5 x 18% + 0.21 x 70%

[2] macle is a common diamond industry term for a crystal twinned on the 111 axis.

# Summary

Zones of heterolithic breccia and lamprophyre dikes were emplaced late in the evolution of the Michipicoten greenstone belt. Available geochronology on zircon and titanite indicates that lamprophyre dikes intruded at 2685 to 2674 Ma approximately concurrent with development of late sedimentary basins and prior to regional folding and plutonism. The undated breccia zones are generally older than lamprophyre dikes but cannot predate 2701 Ma-old cycle 3 volcanic rocks, which occur as xenoliths within the breccia. Consequently, the heterolithic breccia and lamprophyre dikes are mildly deformed and have been metamorphosed to upper greenschist facies. Both contain a common mineral assemblage represented by actinolite+chlorite+epidote+titanite±albite.

Although difficult to distinguish from one another in small outcrops, a variety of field criteria and textural, mineralogical and chemical characteristics can be used to differentiate lamprophyre dikes from breccia zones (Table 11). For example, the lamprophyre dikes tend to be small (<5 m wide) and crosscut the broader breccia units (up to 70 m) although the overall forms of the breccia units are, as yet, poorly defined. The lamprophyres dikes are mainly medium-grained spessartite with a granoblastic to decussate texture whereas the matrix of the breccia units is a fine-grained ultramafic schist. Hornblende macrocrysts are identified only in the breccia matrix whereas feldspar and biotite are more common in the dikes than in the breccia. Enclaves within the lamprophyre dikes are mainly altered ultramafic material whereas mafic to intermediate and felsic supracrustal clasts predominate within the breccias. In terms of chemical composition, the breccia matrix at the Engagement and Cristal occurrences has a higher Mg#, higher transition metals including Cr, Ni and Co and lower REE and LILE than lamprophyre dikes.

Although breccia matrix at the Engagement and Cristal occurrences is chemically primitive compared to lamprophyre dikes, the trace element profiles of the breccia matrix material and lamprophyre dikes are parallel. This suggests that the magma representing the lamprophyre dikes could have evolved from magma characteristic of the breccia matrix through processes such as fractionation, although further work on a larger data set is required for confirmation. At the Oasis occurrence, rock identified on the basis of field relations as breccia is mineralogically and chemically more like the material comprising lamprophyre dikes than the matrix of breccia at the Engagement and Cristal occurrences. This may indicate that the Oasis breccias are lamprophyre dikes or else they represent an intermediate stage in the evolution of magmas from a primitive composition representative of breccia matrix to an evolved composition representative of lamprophyre dikes.

The heavy mineral assemblage of diamondiferous heterolithic breccia matrix is dominated by pyrite, rutile, zircon and titanite. These minerals are common in a wide range of Archean plutonic and supracrustal rocks and cannot be used reliably as indicators of a potentially diamondiferous source. Indeed, heterolithic breccias and lamprophyre dikes contain very little pyrope, picro-ilmenite, chrome diopside and chromite that are the normal indicator minerals of potentially diamondiferous, mantle-derived source rocks. Hence, the standard prospecting procedure of searching for the normal suite of kimberlite indicator minerals in the heavy mineral concentrates of till and modern alluvium samples may be of limited value in detection of new mineralization. Thomas and Gleeson (2000) found elevated concentrations of Ni and Cr in till overlying and down-ice of known lamprophyre dikes in the Wawa area, and that the heavy minerals in till that were most useful included: actinolite, chromite, and ilmenite. However, the most effective prospecting seems to require the identification of lamprophyre dikes and breccia zones through standard surface mapping, trenching, drilling or geophysical methods followed by processing of the dike or breccia material for diamonds. Techniques of magnetic and heavy liquid separation, such as was used here, or caustic dissolution can be applied.

Williams (2002) concluded that diamondiferous lamprophyre dikes are chemically more primitive (higher Mg#, higher transition metals including Cr, Ni and Co and lower REE and LILE) than non-diamondiferous lamprophyre dikes. By extending this correlation between diamond-content and host-rock composition, one would expect that the ultramafic matrix of breccia at the Engagement occurrence, which is chemically more primitive than diamondiferous lamprophyre dikes, should be highly prospective for diamonds but this is not necessarily the case. Two samples of mineralogically and chemically similar breccia matrix produced abundant small diamonds and no diamonds, respectively. Since the processing method was the same for both samples, it appears that diamonds are unevenly distributed in the breccia matrix. Although the bulk compositions of the diamondiferous and non-diamondiferous breccia matrix are very similar, the heavy mineral concentrate is an order of magnitude larger in the diamondiferous material than in the non-diamondiferous material. This suggests that heavy minerals including diamonds could have been locally concentrated within the breccia by an unknown geologic process. Clearly, further work is required to determine the origin of the diamonds and their distribution within the various components of the complex clast-laden lamprophyre dikes and breccia zones.

The heterolithic breccias remain geologically intriguing and poorly understood. Further research is required to establish the form, age and distribution of these features as well as their origin either as intrusive diatreme-like dikes or through volcanic eruption or both. The compositional variation of lamprophyre and breccia material, such as between the Engagement-type and Oasis-type requires further definition and may provide a useful guide to exploration. For example, the bulk composition may correlate with the diamond content of the host material as proposed by Williams (2002). Hence, an evaluation of the bulk composition of a candidate host, through mineralogical or chemical methods, may provide a preliminary assessment of potential diamond content, at lower cost than the direct processing of the material for diamonds.

**Table 11:** Comparison of lamprophyres (02DS98 and 02DS99) with breccia matrix (samples 02DS86, 02DS87 and 02DS89) from the Michipicoten greenstone belt.

| Characteristic | Lamprophyre | Breccia |
|---|---|---|
| Age (Ma) | 2685 to 2674 | 2701 to 2674 |
| Form | Dikes, mainly less than 5 m wide | Complex zones up to 70 m wide |
| Colour | Medium to dark green | Dark green with white clasts |
| Grain Size | Mainly medium-grained | Fine-grained |
| Texture | Granoblastic | Schistose |
| Rock Type | Mainly spessartite | Basaltic komatiite |
| Enclaves | Mainly zoned, rounded and altered ultramafic rocks | Mainly volcanic country rocks |
| Macrocrysts | Amphibole and biotite | Hornblende, actinolite |
| Mineral Assemblage | Actinolite+biotite+albite±chlorite+titanite±epidote±calcite | Actinolite+chlorite+(rare) albite+titanite±epidote±calcite |
| Composition | $SiO_2$=47 to 48%, Mg#=66 to 69, Cr=633 to 720, Rb=81 to 146, $La/Yb_N$=8 to 12, Sum REE=109 to 137. | $SiO_2$=44 to 45%, Mg#=78 to 80, Cr=1292 to 1369, Rb=3 to 9, $La/Yb_N$=8, Sum REE=84 to 88. |
| Heavy Mineral Concentrate | - | Pyrite, rutile, zircon, titanite |

# Acknowledgements

This work was stimulated by a talk given by Ed Walker at the meeting of the Ontario Prospectors Association in Toronto December 2001, in which he described the unusual diamond occurrences at Wawa. We thank Ann Wilson for her guidance in the field and John Ayer, Ron Sage and Christine Vaillancourt for helpful discussions. The manuscript benefited from comments by John Ayer, Jack Parker, Christine Vaillancourt and Ann Wilson.

# References


Arias, Z.G. and Helmstaedt, H. 1990. Structural evolution of the Michipicoten (Wawa) greenstone belt, Superior Province: evidence for an Archean fold and thrust belt; *in* Geoscience Research Grant Program Summary of Research 1989-1990, Ontario Geological Survey, Miscellaneous Paper 150, p. 107-114.

Ayer, J.A., Conceição, R.V., Ketchum, J.W.F., Sage, R.P., Semenyna, L. and Wymann, D.A. 2003. The timing and petrogenesis of diamondiferous lamprophyres in the Michipicoten and Abitibi greenstone belts; *in* Summary of Field Work and Other Activities 2003, Ontario Geological Survey, Open File Report 6120, p. 10-1 to 10-9.

Corfu, F. and Sage, R. 1987. A precise U-Pb zircon age for a trondhjemite clast in Doré conglomerate, Wawa, Ontario; *in* Proceedings and Abstracts, Institute on Lake Superior Geology Annual Meeting, v. 33, p.18.

Corfu, F. and Sage, R. 1992. U-Pb age constraints for deposition of clastic metasedimentary rocks and late-tectonic plutonism, Michipicoten belt, Superior Province; Canadian Journal of Earth Sciences, v. 29, p. 1640-1651.

Deer, W.A., Howie, R.A. and Zussman, J. 1972. An Introduction to the Rock-Forming Minerals; Longman, London, 528p.

Easton, R.M. 2000. Metamorphism of the Canadian Shield, Ontario, Canada. 1. The Superior Province; The Canadian Mineralogist, v. 38, p.287-317.

Irving, T.N. and Baragar, W.R.A. 1971. A guide to the chemical classification of the common volcanic rocks; Canadian Journal of Earth Sciences, v.8, p. 523-548.

Jensen, L.S. 1976. A new cation plot for classifying subalkalic volcanic rocks; Ontario Division of Mines, Miscellaneous Paper 66, 22p.

Ketchum, J., Kamo, S. and Davis, D. 2003. U-Pb ages from the Superior and Grenville Provinces of Ontario; unpublished report of the Jack Satterly Geochronology Laboratory, Toronto, 15p.

Leake, B.E., Woolley, A.R., Arps, C.E.S., Birch, W.D., Gilbert, M.C., Krivovichev, V.G., Linthout, K., Laird, J., Mandarino, J.A., Maresch, W.V., Nickel, E.H., Rock, N.M.S., Schumacher, J.C., Smith, D.C., Stephenson, C.N., Ungaretti, L., Whittacker, E.J.W. and Youzhi, G. 1997. Nomenclature of amphiboles: report of the Subcommittee on Amphiboles of the International Mineralogical Association, Commission on New Minerals and Mineral Names; American Mineralogist, v.82, p.1019-1037.

Lefebvre, N.S., Kopylova, M.G., Kivi, K.R. and Barnett, R.L. 2003. Diamondiferous volcaniclastic debris flows of Wawa, Ontario, Canada; abstract *in* the 8th International Kimberlite Conference, Victoria, p 6-7.

Le Maitre, R.W. 1989. A classification of igneous rocks and glossary of terms: recommendations of the International Union of Geological Sciences Subcommission on the systematics of igneous rocks; Blackwell Scientific Publishing, Oxford, 193p.

Liou, J.G., Kuniyosho, S. and Ito, K. 1974. Experimental studies of the phase relations between greenschist and amphibolite in a basaltic system; American Journal of Science, v. 274, p.613-632.

McCallum, M.E., Huntley, P.M., Falk, R.W. and Otter, M.L. 1991. Morphological, resorption and etch feature trends of diamonds from kimberlite populations within the Colorado-Wyoming State Line District, USA; *in* Diamonds: Characterization, Genesis and Exploration, H.O.A Meyer and O.H. Leonardos (eds.), Proceedings of the Fifth International Kimberlite Conference, Araxa', Brazil, p.32-50.

Menard, T., Ridgeway, C.K., Stowell, H.H. and Lesher, C.M. 1999. Geochemistry and textures of metasomatic combs and orbicules in ultramafic rocks, Namew Lake, Manitoba; Canadian Mineralogist, v.37, p.431-442.

Mitchell, R.H. 1995. Kimberlites, orangeiites, and related rocks; Plenum Press, New York, 410p.

Morris, T.F., Murray, C. and Crabtree, D. 1994. Results of overburden sampling for kimberlite heavy mineral indicators and gold grains, Michipicoten River-Wawa area, northeastern Ontario; Ontario Geological Survey, Open File Report 5908, 69p.

Moody, J.B., Meyer, D. and Jenkins, J.E. 1983. Experimental characteristics of the greenschist/amphibolite boundary in mafic systems; American Journal of Science, v.283, p. 48-92.

Morimoto, N. 1989. Nomenclature of pyroxenes; Canadian Mineralogist, v.27, p.143-156.

Otter, M.L., McCallum, M.E. and Gurney, J.J. 1991. A physical characteristic of the Sloan (Colorado) diamonds using a comprehensive diamond description scheme; *in* Diamonds: Characterization, Genesis and Exploration, H.O.A Meyer and O.H. Leonardos (eds.), Proceedings of the Fifth International Kimberlite Conference, Araxa', Brazil, p.15-31.

Pearce, J.A. 1996. A user's guide to basalt discrimination diagrams; *in* D.A. Wyman ed., Trace Element Geochemistry of Volcanic rocks: Applications for Massive Sulphide Exploration, Geological Association of Canada, Short Course Notes, v. 12, p. 79-114.

Queen, M., Heaman, L.M., Hanes, J.A., Archibald, D.A. and Farrar, E. 1996. $^{40}Ar/^{39}Ar$ phlogopite and U-Pb perovskite dating of lamprophyre dykes from the eastern Lake Superior region: evidence for a 1.14 Ga magmatic precursor to midcontinental rift volcanism; Canadian Journal of Earth Sciences, v. 33, p. 958-965.

Rock, N.M.S. 1991. Lamprophyres; Blackie, London, 285p.

Sage, R. 1994. Geology of the Michipicoten greenstone belt; Ontario Geological Survey, Open File Report 3888, 592p.

—1996. Kimberlites of the Lake Timiskaming Structural Zone; Ontario Geological Survey, Open File Report 5973, 435p.

— 2000a. Kimberlites of the Attawapiskat Area, James Bay Lowlands, Northern Ontario; Ontario Geological Survey, Open File Report 6019, 341p.

— 2000b. The "Sandor" diamond occurrence, Michipicoten greenstone belt, Wawa, Ontario: a preliminary study; Ontario Geological Survey, Open File Report 6016, 49p.

Sage, R. and Crabtree, D. 1997. The "Nicholson" ultramafic dike, Wawa, Ontario: a preliminary investigation; Ontario Geological Survey, Open File Report 5955, 111p.

Santaguida, F. 2001. Precambrian geology compilation series-White River sheet; Ontario Geological Survey, Map 2666, scale 1:250 000.

Schiffman, P. and Liou, J.G. 1980. Synthesis and stability relations of Mg-Al pumpellyite, $Ca_4Al_5MgSi_6O_{21}(OH)_7$; Journal of Petrology, v.21, p.441-474.

Stone, D. 2000. Temperature and pressure variations in suites of Archean felsic plutonic rocks, Berens River area, northwest Superior Province, Ontario, Canada; The Canadian Mineralogist, v.38, p.455-470.

— 2001. A study of indicator minerals for kimberlite, base metals and gold: northern Superior Province of Ontario; Ontario Geological Survey, Open File Report 6066, 140p.

Stott, G.M., Ayer, J.A., Wilson, A.C. and Grabowski, G.P.B. 2002. Are the Neoarchean diamond-bearing breccias in the Wawa area related to late-orogenic alkalic and "sanukitoid" intrusions?; *in* Summary of Field Work and Other Activities 2002, Ontario Geological Survey, Open File Report 6100, p. 9-1 to 9-10.

Sullivan, R.W., Sage, R.P. and Card, K.D. 1985. U-Pb zircon age of the Jubilee stock in the Michipicoten greenstone belt near Wawa, Ontario; *in* Current Research, part B, Geological Survey of Canada, Paper 85-1B, p. 361-365.

Sun, S.-s., and McDonough, W.F. 1989. Chemical and isotopic systematics of oceanic basalts: implications for mantle composition and processes; *in* Magmatism in the Ocean Basins, Geological Society Special Publication no. 42, p. 313-345.

Thomas, R.D. and Gleeson, C.F. 2000. Use of till geochemistry and mineralogy to outline areas underlain by diamondiferous spessartite dikes near Wawa, Ontario; Exploration and Mining Geology, v.9, p.215-231.

Turek, A., Keller, R. and Van Schmus, W.R. 1990. U-Pb zircon ages of volcanism and plutonism in the Mishibishu greenstone belt near Wawa, Ontario; Canadian Journal of Earth Sciences, v. 27, p. 649-656.

Turek, A., Sage, R.P. and Van Schmus, W.R. 1992. Advances in the U-Pb zircon geochronology of the Michipicoten greenstone belt, Superior Province, Ontario; Canadian Journal of Earth Sciences v. 29, p. 1154-1165.

Turek, A., Smith, P.E. and Van Schmus, W.R. 1984. U-Pb zircon ages and evolution of the Michipicoten plutonic-volcanic terrane of the Superior Province, Ontario; Canadian Journal of Earth Sciences, v. 21, p. 457-464.

Vaillancourt, C., Wilson, A. and Dessureau, G.R. 2003. Synthesis of Archean geology and diamond-bearing rocks in the Michipicoten greenstone belt: geology of Menzies Township; *in* Summary of Field Work and Other Activities 2003, Ontario Geological Survey, Open File Report 6120, p. 9-1 to 9-11.

Walker, E. 2003. Diamond exploration at the Festival property, Wawa, Ontario; lecture, Ontario Prospectors Association, Annual Meeting, Toronto, Dec. 9.

Williams, F. 2002. Diamonds in late Archean calc-alkaline lamprophyres Ontario, Canada: origins and implications; unpublished BSc thesis, University of Sydney, 103p.

Wilson, A. 2002. Diamond occurrences of the Wawa area; unpublished field trip guide book, Resident Geologist's Office, Timmins, 14p.

Wyman, D.A. and Kerrich, R. 1993. Archean shoshonitic lamprophyres of the Abitibi Subprovince, Canada: petrogenesis, age and tectonic setting; Journal of Petrology, v. 34, p.1067-1109.

# Metric Conversion Table

| Conversion from SI to Imperial | | | Conversion from Imperial to SI | | |
|---|---|---|---|---|---|
| *SI Unit* | *Multiplied by* | *Gives* | *Imperial Unit* | *Multiplied by* | *Gives* |
| | | LENGTH | | | |
| 1 mm | 0.039 37 | inches | 1 inch | **25.4** | mm |
| 1 cm | 0.393 70 | inches | 1 inch | **2.54** | cm |
| 1 m | 3.280 84 | feet | 1 foot | **0.304 8** | m |
| 1 m | 0.049 709 | chains | 1 chain | 20.116 8 | m |
| 1 km | 0.621 371 | miles (statute) | 1 mile (statute) | **1.609 344** | km |
| | | AREA | | | |
| 1 $cm^2$ | 0.155 0 | square inches | 1 square inch | **6.451 6** | $cm^2$ |
| 1 $m^2$ | 10.763 9 | square feet | 1 square foot | **0.092 903 04** | $m^2$ |
| 1 $km^2$ | 0.386 10 | square miles | 1 square mile | 2.589 988 | $km^2$ |
| 1 ha | 2.471 054 | acres | 1 acre | 0.404 685 6 | ha |
| | | VOLUME | | | |
| 1 $cm^3$ | 0.061 023 | cubic inches | 1 cubic inch | **16.387 064** | $cm^3$ |
| 1 $m^3$ | 35.314 7 | cubic feet | 1 cubic foot | 0.028 316 85 | $m^3$ |
| 1 $m^3$ | 1.307 951 | cubic yards | 1 cubic yard | 0.764 554 86 | $m^3$ |
| | | CAPACITY | | | |
| 1 L | 1.759 755 | pints | 1 pint | 0.568 261 | L |
| 1 L | 0.879 877 | quarts | 1 quart | 1.136 522 | L |
| 1 L | 0.219 969 | gallons | 1 gallon | **4.546 090** | L |
| | | MASS | | | |
| 1 g | 0.035 273 962 | ounces (avdp) | 1 ounce (avdp) | 28.349 523 | g |
| 1 g | 0.032 150 747 | ounces (troy) | 1 ounce (troy) | **31.103 476 8** | g |
| 1 kg | 2.204 622 6 | pounds (avdp) | 1 pound (avdp) | **0.453 592 37** | kg |
| 1 kg | 0.001 102 3 | tons (short) | 1 ton (short) | **907.184 74** | kg |
| 1 t | 1.102 311 3 | tons (short) | 1 ton (short) | **0.907 184 74** | t |
| 1 kg | 0.000 984 21 | tons (long) | 1 ton (long) | **1016.046 908 8** | kg |
| 1 t | 0.984 206 5 | tons (long) | 1 ton (long) | **1.016 046 90** | t |
| | | CONCENTRATION | | | |
| 1 g/t | 0.029 166 6 | ounce (troy)/ ton (short) | 1 ounce (troy)/ ton (short) | 34.285 714 2 | g/t |
| 1 g/t | 0.583 333 33 | pennyweights/ ton (short) | 1 pennyweight/ ton (short) | 1.714 285 7 | g/t |

OTHER USEFUL CONVERSION FACTORS

| | *Multiplied by* | |
|---|---|---|
| 1 ounce (troy) per ton (short) | 31.103 477 | grams per ton (short) |
| 1 gram per ton (short) | 0.032 151 | ounces (troy) per ton (short) |
| 1 ounce (troy) per ton (short) | 20.0 | pennyweights per ton (short) |
| 1 pennyweight per ton (short) | 0.05 | ounces (troy) per ton (short) |

*Note: Conversion factors which are in bold type are exact. The conversion factors have been taken from or have been derived from factors given in the Metric Practice Guide for the Canadian Mining and Metallurgical Industries, published by the Mining Association of Canada in co-operation with the Coal Association of Canada.*

ISSN 0826-9580
ISBN 0-7794-5902-4